WAVE GENERATION AND ANALYSIS IN THE LABORATORY WAVE CHANNEL TO CONDUCT EXPERIMENTS ON THE NUMERICALLY MODELED SPAR TYPE FLOATING WIND TURBINE

A Thesis Submitted to
the Graduate School of Engineering and Sciences of
İzmir Institute of Technology
in Partial Fulfillment of the Requirements for the Degree of

MASTER OF SCIENCE

in Civil Engineering

by
Kadir AKTAŞ

December 2020
İZMİR

ACKNOWLEDGMENTS

I would like to express my deepest gratitude to my dear advisor Assoc. Prof. Dr. Bergüzar Özbahçeci for the guidance and support she provided through my M.Sc. study. This thesis is written thanks to her being the most patient mentor a student can ask for. imparting her knowledge and expertise in this study. Also, I thank her for providing opportunities such as sharing some findings of this work at the national conference "9. Kıyı Mühendisliği Sempozyumu" held in Adana, November 2018.

Besides my advisor, I would like to thank Assoc. Prof. Dr. Ünver Özkol for allowing me to work on this astonishing project and become a part of this great team.

This study was funded by the Scientific and Technological Research Council of Turkey, TUBITAK under 217M451.

I would like to send my sincere gratitude to my colleague Ruwad Adnan Al Karem who provided the design for the spar platform model.

Also, I would like to thank Bahadır Öztürk for opening up his house whenever I had to stay late studying, and to thank Hazal Emet and Cemal Kılıç for the help they provided in the laboratory.

I would like to thank my father, Mehmet Aktaş, for teaching me perseverance.

Lastly, I would like to thank my mother, Gülnur Ölçer, who passed the passion for knowledge down to her son.

To my wife, Emel Aktaş

ABSTRACT

WAVE GENERATION AND ANALYSIS IN THE LABORATORY WAVE CHANNEL TO CONDUCT EXPERIMENTS ON THE NUMERICALLY MODELED SPAR TYPE FLOATING WIND TURBINE

The oceans offer immense potential for harvesting sustainable wind energy, with stronger and steadier winds for locations further offshore. Since the feasibility of fixed-bottom offshore wind turbines decreases with increasing water depth, floating offshore wind turbines (FOWT) becomes a promising field of study.

As part of a TÜBİTAK project (217M451) that investigates the dynamic performance of different FOWT designs under wind and wave loads, the necessary laboratory wave generation, analysis, and test set-up to conduct physical model experiments of a spar-type FOWT model is established in this study. An investigation of the wavemaker theory yielded that using first-order wavemaker solutions in the laboratory leads to the generation of spurious harmonic waves that do not appear in natural waves. Therefore, the second-order solutions are applied to the piston-type wave generator for a closer approximation of natural waves in laboratory conditions.

A numerical model investigation of a reference spar-type FOWT is conducted to gain insights into spar design using ANSYS AQWA. The results indicate that the spar model dynamic responses are susceptible to low-frequency waves in pitch and surge degrees of freedom as its natural frequency lies in that region which further emphasizes the importance of generating laboratory waves using second-order wavemaker theory. Additionally, a spar-type floating platform is modeled at the 1/40 Froude scale, to use in the hydraulic model experiments. The wave measurement set-up is fully implemented and theoretically generated waves are measured for validation. In conclusion, regular and irregular wave generation and wave analysis in the time and the frequency domain could be possible in the wave channel of IZTECH Civil Engineering Hydraulic Laboratory.

ÖZET

SAYISAL OLARAK MODELLENEN SPAR TİPİ YÜZER RÜZGAR TÜRBİNİNİN FİZİKSEL MODEL DENEYLERİ İÇİN LABORATUVARDA DALGA ÜRETİMİ VE ANALİZİ

Açık denizler karaya kıyasla daha yüksek ve sürekli rüzgar profilleri göstermesi ile sürdürebilir rüzgar enerjisi sektöründe yükselişini sürdürmektedir. Sabit tabanlı açık deniz rüzgar türbinlerinin enerji potansiyelinin daha yüksek olduğu karadan uzak ve derin bölgelerde elverişsiz olması ile yüzer rüzgar türbinlerinin önemi artmaktadır.

Bu çalışmada 217M451 kodlu TÜBİTAK projesi kapsamında sayısal modellemesi yapılmış spar tipi bir yüzer rüzgar türbinin fiziksel deneylerini gerçekleştirmek amacıyla İYTE Hidrolik Laboratuvarındaki dalga kanalına yerleştirilmiş piston tipi dalga üretecinin doğradaki düzensiz dalgalara benzer dalga serileri üretmesi sağlanmıştır. Teorik bir spektruma uygun rastgele dalga zaman serileri oluşturulup bu dalgaları laboratuvar dalga kanalında elde etmek için gereken zamana bağlı dalga pedalı konumları ikinci mertebe transfer fonksyonları ile hesaplanmış, pedal hareketiyle oluşturulan dalgalar kanala yerleştirilen dalga ölçerler yardımıyla okunmuştur. Oluşturulan teorik dalgalar matematiksel analiz yöntemleri ile ve dalga üretecinin ürettiği dalgalar laboratouvar ölçümleri ile doğrulanmıştır.

Ayrıca spar tipi bir platformun ANSYS AQWA programında nümerik modellenmesi yapılmış, düşük frekanslı dalgaların platform tepkilerine yüksek ölçüde etkisi olduğu gözlemlenmiştir. Proje kapsamında incelenecek olan spar tipi yüzer rüzgar türbinin platformu, 1:40 Froude ölçeği kullanarak modellenmiş ve imal edilmiştir. Sonuç olarak İYTE Hidrolik Laboratuvarı dalga kanalında ikinci dereceden düzenli ve düzensiz dalgalar üretilmiş, kullanılan metodlar doğrulanmış ve fiziksel model deneyleri için gerekli hazırlıklar tamamlanmıştır.

TABLE OF CONTENTS

LIST OF FIGURES

Figure **Page**

Figure **Page**

LIST OF TABLES

Table **Page**

CHAPTER 1

INTRODUCTION

1.1. Research Setting & Background

Wind energy is a much sought-after form of sustainable, clean energy due to its low impact on the environment, low emission of carbon and other harmful substances, and due to it not relying on fuel and freshwater. The global installed capacity of wind energy shows a steady increase for nearly twenty years (GWEC 2019). However, there is a tendency towards offshore wind energy lately in the market.

The offshore wind energy potential is often associated with stronger and steadier wind characteristics, which provides the advantages of an increased energy yield and longer operating life. This effect becomes more and more pronounced for locations further offshore. Offshore wind turbines with foundations that are fixed to the seabed are installed in the initial efforts to harvest the offshore wind energy. However, to benefit more from the energy potential of offshore winds, as well as to avoid complications such as visually polluting the urban areas or damaging the local fauna and flora, the investments and the research efforts displayed a shift towards further offshore and, by extension, deeper waters. Fixed-bottom offshore wind turbines cease being feasible in deeper waters, which led to the development of floating offshore wind turbines (FOWT).

A floating offshore wind turbine can be described as a wind turbine mounted on a floating platform, which can maintain stability and keep stationary under the wind, wave, and current loads by using any combination of ballast, buoyancy, and taut or catenary mooring lines. The performance and safety are directly related to the stability and station-keeping abilities of the FOWT. Several FOWT design concepts gained prominence in that regard, such as the spar-buoy concept, which mainly uses ballast weight and high draft, the semi-submersible concept, which mostly takes advantage of a large water-plane area and ballast weight, and the tension-leg platform (TLP), which makes use of taut mooring lines that anchor the platform to the seabed, to achieve

stability. Figure 1.1 provides the example platform models that use these stabilization schemes.

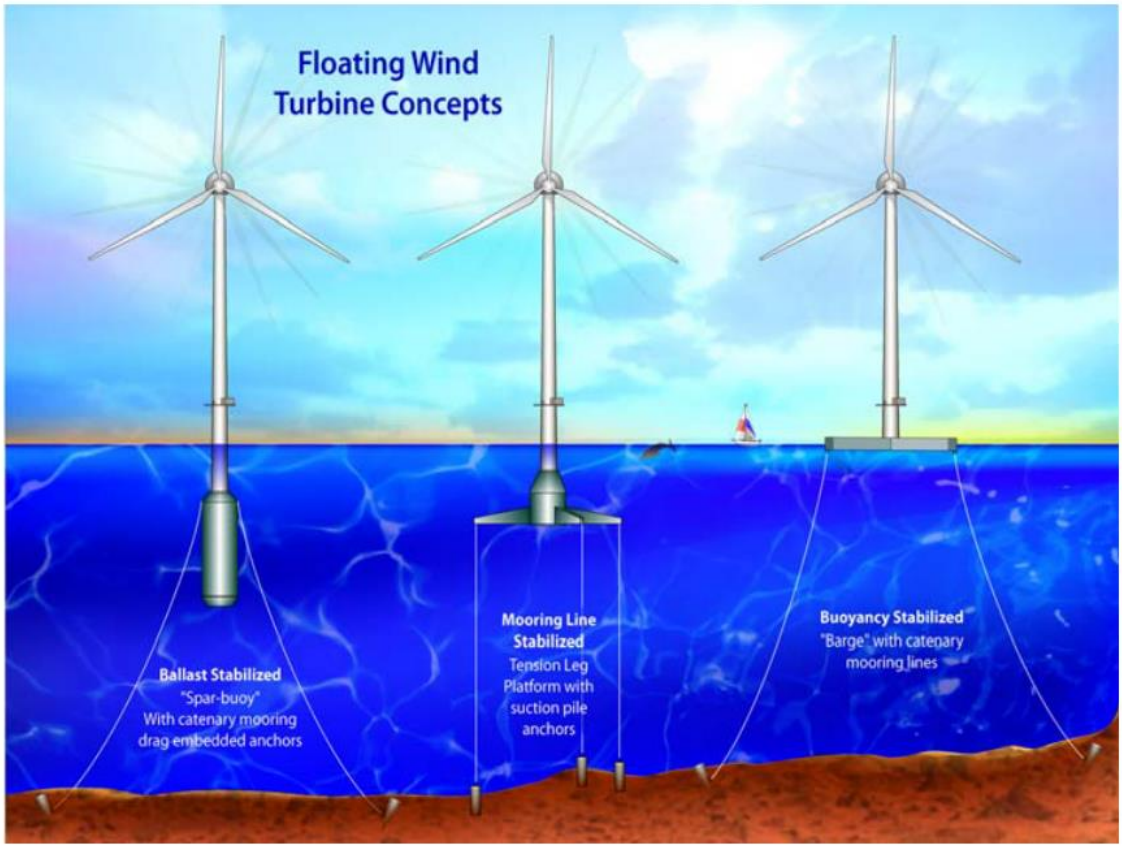

Figure 1.1: Three different FOWT concepts
(source: Butterfield et al. 2005)

In tandem with the research efforts on the subject, offshore wind energy investments soared globally with the cumulative installed capacity tripling between 2010 and 2019, and a projected increase of another sixfold by 2030. However, to this day, offshore wind energy remains a small portion of the wind energy industry and there is so much room for research regarding the design, optimization, and development of floating offshore wind turbines.

Physical model experiments have a wide-spread use in the research of floating offshore wind turbines. They provide means to test, calibrate, and validate the performance and feasibility of a design and are especially useful when complemented with numerical model studies. Large-scale physical experiments usually require a great deal of funding and workforce, and a research field such as floating offshore wind turbines is not an exception. However, a physical system can be represented as a small-

scale model, which can demonstrate similar behavior to the prototype under the same environmental loads. The laws of similitude apply in the scale-model experiments, which are essential to relate the model and the prototype to each other. The way to achieve similitude in physical experiments is to keep a dimensionless parameter constant in the model and the prototype. In the experiments concerning FOWTs, the main problem is achieving stability, and the main environmental loads acting on the structure is the wave loads, which are mostly associated with inertial and gravitational forces, so Froude number is used as the scaling criterion, which gives the ratio of inertial and gravitational forces. However, a comprehensive physical model of a FOWT will also require the wind loads to be taken into account, which is best represented with Reynold's number as the scaling criterion. This discrepancy is usually compensated by keeping the wind force to wave force (alternatively, wind speed to wave celerity) ratio constant, as well as maintaining the wind turbine tip speed ratio (TSR) between the model and the prototype (Martin et al. 2014a).

Wave reproduction in the laboratory wave channel is essential to conduct physical model experiments. In older times only regular waves that have constant wave height and period could be produced in the laboratories. However, regular waves do not represent the real waves that are irregular with different wave height and the period in a time series in nature. Developments in the wavemaker theory and technology made it possible to reproduce irregular waves in the laboratory. Yet, there are only a few laboratories in the world that are capable of irregular wave generation.

1.2. Aim and Scope of the Study

This study aims to provide an appropriate laboratory setup for the physical model experiments of floating offshore wind turbines including the development of a wave generator capable of reproducing both regular and irregular waves; wave analysis in the time and the frequency domain in the laboratory wave flume. The main objectives are as follows:

1- the numerical investigation of the hydrodynamic behavior of a reference spar-type FOWT

2- the synthesis of irregular wave series that are representative of those encountered in nature
3- the calculation of the wave board motion that can reproduce the second-order waves correctly for a piston-type wave generator
4- the production of a physical model of a numerically tested spar-type FOWT design.
5- the establishment of the laboratory set-up required to conduct physical model experiments of the FOWT model in the future
6- Wave reflection analysis

The wave flume at IZTECH Hydromechanics Laboratory is used in this study, which allows the generation of unidirectional waves. It means that the enabled degrees of freedom (DOFs) for the FOWT will be surge, heave, and pitch in future physical experiments. Therefore, the same DOFs are investigated in the numerical study given in chapter 3. The six degrees of freedom for floating structures are shown in Figure 1.2.

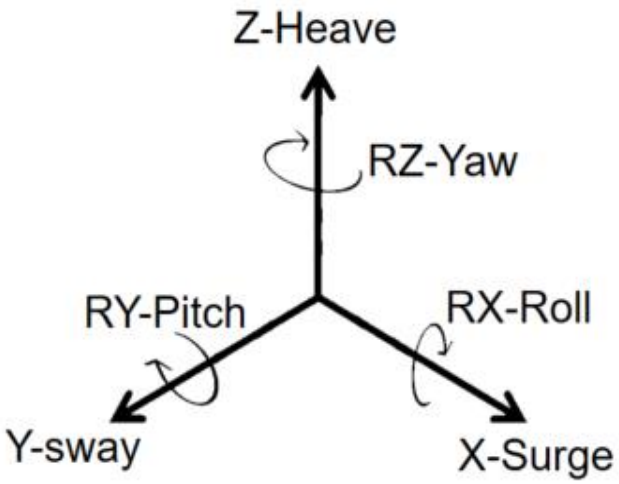

Figure 1.2: The six degrees of freedom of rotations and translations

Any efforts involving the generation of the wind and correspondingly, the production of the upper structure of the FOWT which consists of the tower, hub, and blades are kept out of scope, as well as the mechanical design of the piston-type wave generator and the conversion of the calculated wave board motions to the corresponding electrical signals for the wave generator.

1.3. The Structure of the Thesis

The thesis consists of the following chapters; a literature review on the FOWTs, wavemaker theory, and wave generation in laboratory conditions is given in Chapter 2. A numerical model study on the hydrodynamic response of a reference spar-type floating offshore wind turbine under wave loads is conducted and the results are provided in Chapter 3. The complete wavemaker theory is provided, and the methods to generate regular and irregular waves correct to the second-order are given in Chapter 4. The laboratory setup for the physical model tests for FOWTs is described and validations to the theoretically generated waves are supplied with wave measurements taken in the wave flume in Chapter 5. The conclusions are drawn from the study, with the description of the limitations, and the recommendations for the next stages in the laboratory experiments are provided in Chapter 6.

CHAPTER 2

LITERATURE REVIEW

Global wind energy harvest is a consistently growing sector (GWEC 2019) and the oceans offer a vast energy potential. Due to the low surface tension, steadier and stronger winds are encountered on open seas (Landberg 2016), providing advantages such as a more efficient energy harvest and longer service life for the wind turbines (Snyder and Kaiser 2009). For the locations near shore, fixed-bottom offshore wind turbines are practical, yet, they cease to be feasible for waters deeper than thirty meters. To access the potentially more profitable open seas, floating offshore wind turbines should be used. For more than a decade, the potential in offshore wind energy is realized and the sector is growing rapidly, with a projected increase of another sixfold in less than a decade (BNEF 2018).

The main research problem in floating offshore wind turbine studies is the dynamic stability performance of the structure. Physical model experiments offer a good approach to investigate the stability of the floating offshore wind turbines under wind and wave loads. Conducting scale model experiments rather than full-scale prototype experiments is often cheaper and more practical (Chakrabarti 1995). To approximate natural environmental loads in laboratory conditions, the proper generation of naturally occurring waves is more than a necessity. Therefore, producing a wave generator becomes a necessity to conduct physical model experiments.

2.1. Wavemakers

The wavemaker theory is a long-studied subject. Stokes (1880) defined wave profiles with velocity potentials as parameters of perturbation series, where wave steepness is chosen as the small ordering parameter. Biesel (1951) defined the first-order transfer function that gives the relation between the displacement of a piston-type wave board and the produced waveform. The velocity profile of a fluid flow in nature can be described with a parabolic function, whereas in the laboratory conditions, the

velocity profile of a planar wave board will be uniform. The concept of velocity profile mismatch and the resulting second-order effects are also pointed out there. Ursell, Dean, and Yu (1960) made efforts to validate the first-order theory in an experimental setup for the first time, using a piston-type wave generator in a laboratory wave flume. Although the accuracy of the results was limited by the reflection in their setup, conclusive results were achieved nonetheless, with less than four percent experimental error. Fontanet (1961) developed a second-order approximation for regular waves by using the Lagrangian approach. He noted the spurious superharmonics generated by the oscillation of the wave board and proposed to suppress them by adding a second-order superharmonic component to the first order wavemaker signal. The generation of spurious harmonic waves in laboratory conditions is of great importance and researchers have conducted extensive studies tackling this problem and those will be mentioned later on. Sulisz and Hudspeth (1993) provided an Eulerian theory by presenting eigenvalue solutions correct to the second order for the fluid motion generated by the monochromatic sinusiodal motion of a wavemaker.

First-order wavemaker theory, when used in two-dimensional laboratory flumes, generates additional free waves that are not originally in the control signal. Those waves are not bound to the wave groups and move freely instead, at their own celerity. That behavior may sometimes reflect and act to cancel the bound harmonic waves naturally traveling with the wave group and sometimes may enhance the amplitude of the bound harmonic waves. Those waves are called “the spurious-free waves” and have to be dealt with to generate proper time series in the laboratory conditions.

There are three types of spurious waves (Barthel et al. 1983). “Parasitic free waves” occur due to boundary conditions of the first order wavemaker theory not meeting the requirements of the second-order bound wave. When the backward component of the orbital velocity of bound wave troughs comes in contact with the wave board, it is reflected with the same phase but a smaller, opposite amplitude. The first-order wavemaker theory boundary condition assumes very small displacements for the wave board, in reality, however, it makes finite oscillations about its mean position. That gives rise to the spurious long waves that are conveniently termed as “displacement free waves”. Finally, “local disturbance-free waves” are generated by evanescent modes that decay exponentially in the wavemaker theory.

It is important to note that in second-order wavemaker theory, waves are often described in terms of bichromatic waves that consist of the difference or the summation of each possible interacting frequency pairs that are in the targeted wave spectrum. These terms are termed as “subharmonic” and “superharmonic”, respectively (Mansard 1988). Subharmonic terms are used to describe long waves and superharmonic terms to describe second-order higher harmonic effects.

Ottesen-Hansen (1978) defined a method to quantify subharmonic and superharmonic effects without the assumption of a narrow banded spectrum by deriving a transfer function in which second-order harmonic contributions are written in terms of interacting first order components. Flick and Guza (1980) theoretically defined first-order theory in laboratory conditions that will produce spurious harmonic waves, they verified this statement with laboratory experiments. Ottesen-Hansen et al. (1980) investigated spurious long waves when irregular waves are generated using the first-order wavemaker theory. The study remarked that the longwave energy plays an important role when the oscillation of moored bodies is of concern to the laboratory setup. Furthermore, a second-order method for a piston-type wavemaker is derived that, when superposed with the first-order wave signal, would eliminate the so-called ‘parasitic’ component of long waves. Additionally, an alternative approach is proposed in the laboratory setup which utilizes shoaling properties of the waves to reduce parasitic wave influence. A complete method to eliminate spurious subharmonic free waves is provided in Sand (1982). The method provides means to calculate second-order compensation signals for each spurious long wave to be added to the first order wavemaker signal.

In nature, irregular wave trains often have nonlinear aspects due to the higher harmonic waves that are bound to the wave group. Second-order higher harmonics alters the wave train in a way that produces steeper wave crests and flatter wave throughs. First-order wavemaker theory comes short with the generation of nonlinear features of a wave train. Sand and Mansard (1986) derived a method for laboratory generation of the higher harmonics while eliminating the spurious superharmonic free waves.

Later, Schäffer (1996) derived a full second-order wavemaker theory. The theory includes both subharmonic and superharmonic corrections in the second-order

and can be used with both rotational and/or translational wavemaker types. In the second-order solutions, infinite summation terms related to the evanescent modes appear. To save computation time, an asymptotic summation method developed by Schäffer (1994) is utilized. This method is also adopted in this study due to its efficient computation scheme and complete secondary harmonic correction techniques. The theory is later extended for multidirectional waves in three-dimensional laboratory basins (Schäffer and Steenberg 2003).

A different approach was developed by Spinneken and Swan (2009a) to wavemaker theory. Instead of the usual position-controlled wavemaker approach, they used force feedback control. The paper reports that force-controlled wavemakers produce less pronounced second-order spurious waves and it also provides a method to eliminate the remaining spurious waves. However, the study is limited to the flap-type wave generators and regular wave cases. Spinneken and Swan (2009b) validate the force feedback control method with experimental data.

There are several approaches when it comes to the shape of the wavemaker and the underlying principle of its motion. One of the earliest, perhaps the most common, types are piston and flap which are planar in shape and they force the waveform by utilizing their oscillatory motion. The aforementioned scholars Biesel (1951), and Ursell, Dean, and Yu (1960) both used piston-type wave generators in their experiments Gilbert, Thompson, and Brewer (1971) provided design curves for piston and flap-type wave generators, Hughes (1993) gave a good comparison of piston and flap-type wave generators as the wave height to stroke ratio being a function of wavenumber and depth. It can be deduced from the comparison that piston wavemakers are more efficient in regards to the amount of stroke needed to produce the same height of waves. On the other hand, it was often argued that flap-type wave generators give a closer representation to the parabolic shape of the natural velocity profile of fluids in deep water waves and piston-type wave generators give a closer approximation to that of shallow waters (Dean and Dalrymple 1984) but that velocity mismatch was proved to cause second-order harmonic effects in every type of wave generators and the problem of elimination of these spurious effects has been tackled extensively in later studies. Hyun (1976) analyzed the first-order solution for a wedge type wave board hinged at a depth above an arbitrary distance from the channel bed, also known as the plunger-type

wave generator. The distinctive property of plunger type wavemakers is that instead of the usual horizontal motions of the wave board, it forces the formation of waves by vertical motions of a wedge-shaped wave board. The mathematical description of the waves generated by a plunger-type wavemaker for general shapes in deep water conditions is given by Wang (1974), describing the generated waves as a function of plunger period and stroke. Wu (1988) later improved the theory using a semi-analytical method and also incorporating the effects of the water depth. Since there are many types of wavemakers a choice can be made considering the research problem, laboratory conditions, wave cases, and wavemaker theory being used (and cost, if necessary).

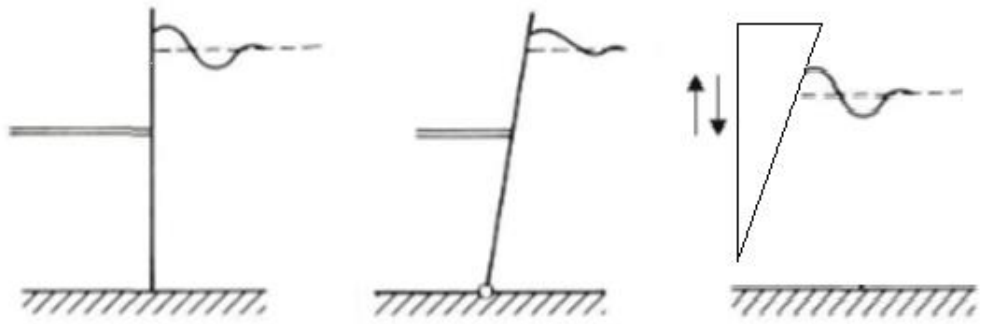

Figure 2.1: A sketch of piston (left), flap (middle), and plunger (right) wavemakers (source: Sand and Donslund 1985)

2.2. Synthesis of Random Waves

To create valid signals for the wavemaker, irregular wave time series must be generated synthetically. There are a lot of established wave generation schemes but the most prevalent ones can be classified under those three approaches: Nondeterministic wave synthesis, deterministic wave synthesis, white noise filtering. The nondeterministic wave synthesis approach, as the name suggests, uses nondeterministic phases and amplitudes, therefore the synthesized wave series will not produce the target spectrum directly (Tuah and Hudspeth 1982). This behavior is analogous to the real ocean waves. To approach the target spectrum, a large number of synthesized waves should be averaged (Funke, Mansard, and Dai 1988). A well-known example of this

approach is the ‘random complex spectrum method (nondeterministic spectral amplitude model)’, which uses Fourier coefficients *‘a’* and *‘b’* that are set randomly, adhering to a Gaussian distribution with zero mean and unit variance. The created spectrum is then multiplied by the square root of the function of the target spectrum, then inverse Fourier transform is applied to generate the time series (Miles and Funke 1989).

Deterministic wave synthesis approach models a Gaussian distribution of wave heights as well as the representation of wave energies by an energy spectrum. Moreover, this approach makes it possible to acquire the exact target spectrum in the synthesized waves. One can argue that this is not analogous to the real ocean behavior but engineers using this type of wave synthesis models have the freedom to have more control over the properties of generated waves. An example of this approach by Goda (1970) is named the random phase method (‘deterministic spectral amplitude model’) where the Fourier components are derived from a target spectrum, using random phases ranged between 0 to 2π. Random wave time series are synthesized using the inverse Fourier Transform. An advantage of this method is that if a pseudorandom number generation algorithm is used in the random phase generation scheme, the same time series can be generated by remembering the ‘seed’.

The white noise filtering approach makes use of the generation of random number series (white noise) that have a uniform or Gaussian probability distribution. An advantage of this approach is that since the pseudorandom number generators’ capacity to generate number sequences that are non-recurring are virtually infinite, the target spectrum can be approximated as a continuous function rather than a set of finite discrete frequencies. Samii and Vandiver (1984) provided a method using this approach where generated white noise sequences are digitally filtered to acquire a time series that matches their targeted Bretschneider spectrum. Miles and Funke (1988) numerically investigated seven wave synthesis methods that fall under those three approaches and concluded that the differences in the mean values and the standard deviations of the wave parameters are insignificant between those methods. If the number of discrete frequencies used is sufficient, synthesis methods involving inverse FFT procedures will be quite realistic as the wave records will be non-recurring. Therefore the researcher is

free to choose one of those methods according to their needs in computation time and convenience.

Another important aspect of creating a random wave series is the assumption of a wave spectrum. According to the needs of the research, adopted spectra should give a good representation of the investigated environment. If the problem can be described, for example, by wind developed waves with the influence of swell generated by remote storms, a representative frequency spectrum would probably have more than one peak whereas a single-peaked spectrum can represent conditions where swell becomes dominated by high, storm waves (Goda, 1999). As the long term wave recordings at single points proliferated, several models of ocean wave spectra have been developed. Pierson and Moskowitz (1964) gave the famous Pierson-Moskowitz spectrum for fully developed oceans at wind speeds observed at 19.5m heights. Using a wide range of locations for measurement, Bretschneider (1959) developed a spectrum with the assumption of a linear correlation between wave height and period squared. By modifying the function factoring in the significant height and period, and their relation to wave spectrum, Mitsuyasu (1970) reformed the function known as the Bretschneider-Mitsuyasu spectrum. Due to observations in the program called Joint North Sea Wave Project spectra of waves where the fetch is limited and the winds are strong show characteristically sharp peaks. Hasselmann (1973) developed the JONSWAP spectrum by keeping the dimensionless fetch as the main parameter and introducing a peak enhancement factor to better achieve a better correlation to the phenomenon. Later, Goda (1988) expressed the spectrum in terms of the significant wave height and peak period. Based on the wind-wave coupled simulations at NASA Wallops Flight Center, Huang et al. (1981) observed that the high-frequency end of the spectrum has, most of the time, a different slope than proposed in the earlier studies, especially when the winds are relatively weak. This led to the definition of the model called the Wallops spectrum, which is later expressed by Goda (1988) in terms of the significant wave height and peak period. Bouws et al. (1985) proposed the TMA spectrum for finite depth cases. Their model gives milder slopes in the high-frequency end of the spectrum, which is better suited to be used in shallow water conditions.

CHAPTER 3

HYDRODYNAMIC MODELING OF THE SPAR-TYPE PLATFORM FOR A FLOATING OFFSHORE WIND TURBINE

3.1. An Overview on Numerical Model and OC3 Offshore Code Comparison Study

There are several platform types for FOWTs that each adopts a different approach to achieve stability. The most popular ones include; spar-type platforms, semi-submersible platforms, and tension-leg platforms (Butterfield et al. 2005). In this study spar, type floating platform is used since it has applications in the world with known properties. Before the physical model experiment stage, to investigate the hydrodynamic behavior of the FOWT with a spar type platform, a numerical model study is carried out.

The ANSYS™ AQWA® package is used in the numerical modeling, which allows the user to simulate the motion of the floating structure in the time domain and provides tools for the investigation of the structural responses in the frequency domain. For hydrodynamic models, the AQWA package offers potential flow or Morison's equation-based applications. Structure response in time and frequency domain is solved under hydrodynamic forces such as inertia forces, drag forces, Froude-Krylov forces, and diffraction forces. Typically, two systems used in the analysis of a floating structure (Aqwa 2013):

1- A hydrodynamic diffraction system is used to calculate hydrostatic analysis of the structure. The definition of load cases consisting of regular or irregular waves is possible, which allows the modeling of wave forces for diffracting structures.

2- A hydrodynamic response system is used, taking the parameters and solutions in the hydrodynamic diffraction system as input, to obtain dynamic

response analysis of the structure in time and/or frequency domain. The system also allows the definition of mooring line connections and calculation of the time or frequency domain performance analysis of such elements.

A spar-type FOWT model is defined in Jonkman (2010) for a numerical code collaboration study named OC3 with participants from 18 countries and results are presented in (Jonkman and Musial 2010). Some of the participants' models and the theories behind their models are provided for comparison with the numerical model in this study in Table 3.1.

Table 3.1: Overview of participants' models

Model	FAST	ADAMS	HAWC2	3Dfloat	Simo
Participant	NREL	NREL+LUH	Risø-DTU	IFE-UMB	MARINTEK
Hydrodynamic Theory	Airy+ME+PF	Airy+ME+PF	Airy+ME	Airy+ME	Airy+PF+ME
Airy: Airy wave theory with free surface connections ME: Morison Equation PF: Linear potential flow with radiation and diffraction					
NREL: National Renewable Energy Laboratory LUH: Leibniz University of Hannover Risø-DTU: Risø National Laboratory of the Technical University of Denmark IFE: Institute for Energy Technology UMB: Norwegian University of Life Sciences					

The OC3 program consists of four development phases of modeling; first, a fixed monopile model with a rigid foundation, second, the same monopile model with flexible foundation, third a tripod-support structure model, and, at the fourth phase, the spar-type floating structure modeled using the Hywind® spar concept. Since a spar-type FOWT is aimed to be modeled for laboratory experiments in this study, the OC3 code collaboration phase 4 is taken as a reference for the numerical model study. The load cases provided in OC3 consist of static analysis of the structure with no environmental loads, free-decay test with no environmental loads, time and frequency domain response analysis under wave load only, and time and frequency domain response analysis under

coupled wind-wave loads. The load cases for the AQWA model are chosen as the static analysis with no loads and environmental wave-only load cases. Any wind-wave coupled load cases are excluded from the model, and the wind turbine is assumed rigid, with the blades locked. The summary of the load cases are given in Table 3.2 preserving the load case indices provided in OC3 phase 4:

Table 3.2: OC3 load-case simulations

Load Case (LC)	**Wind Conditions**	**Wave Conditions**	**Analysis Type**
1.2	None: $\rho_{air} = 0$	Still water	Eigenanalysis
1.3	None: $\rho_{air} = 0$	Still water	Static Equilibrium solution
1.4	None: $\rho_{air} = 0$	Still water	Free-decay test time series
4.1	None: $\rho_{air} = 0$	Regular Airy: $H = 6\ m, T = 10\ s$	Periodic time-series solution
4.1	None: $\rho_{air} = 0$	Irregular Airy: $H_s = 6\ m, T_p = 10\ s$ JONSWAP wave spectrum	Time-series statistics, power spectra

3.2. Modeling of a Spar-Type Floating Platform

Spar-type platforms are floating structures with a deep draft that use a ballast-stability scheme, which achieves stability using the ballast that lowers the center of gravity of the structure below the center of buoyancy and creates a righting-moment that counters the excitations on the structure and forces it to its initial, static equilibrium position. Hywind spar-type FOWT is modeled following the offshore code collaboration project, OC3 (Jonkman and Musial 2010). The platform as it is modeled in AQWA® is given in Figure 3.1**.** In the original Hywind® concept there are three catenary lines attached to the platform via a delta connection and each line consists of multiple segments of varying properties (Jonkman 2010). However, due to this design needlessly complicating the numerical modeling of the catenary lines, the segments with different properties are converted to a unified catenary cable with adjusted properties (cable length, cable stiffness) that are representative of the previous

connection, and the delta connection is eliminated (Jonkman 2010). However, the delta connection added yaw stiffness to the platform and additional yaw stiffness is added to the AQWA model to compensate for the elimination of the delta connection.

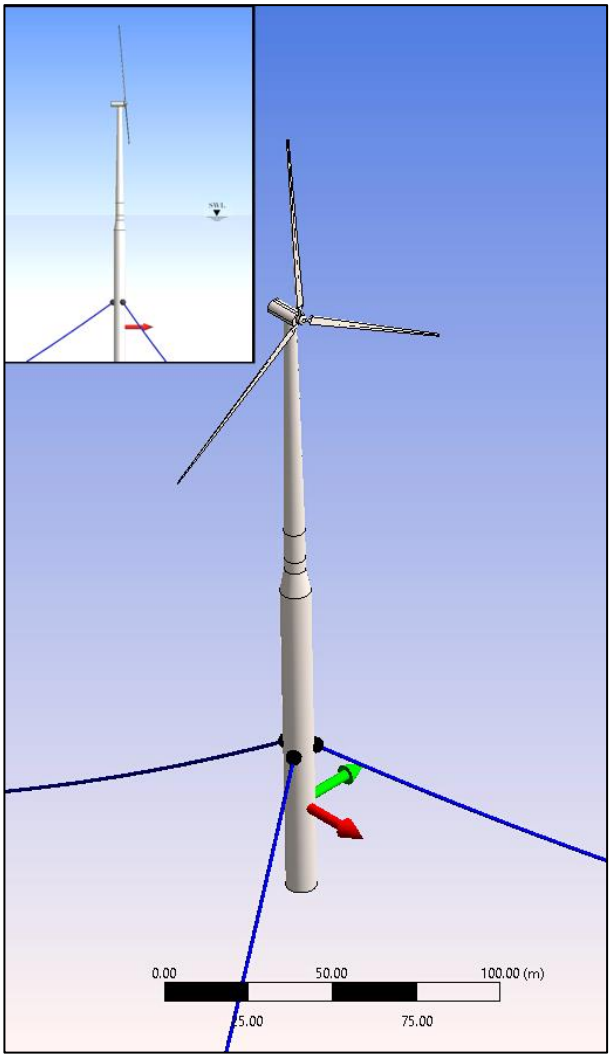

Figure 3.1: Spar-type FOWT modeled in AQWA®

The structural properties such as moments of inertia in six degrees of freedom are given in the paper, therefore the mechanical calculations of such properties were not necessary for the modeling process. The model operates at a water depth of 320 meters, with a draft of 120 meters. The geometry of the platform is modeled according to the provided values. Platform mass was given and it was represented as a point load in the AQWA model. The wind turbine was also represented as a point load with a downward vector at the location of the center of mass of the wind turbine. Properties of the spar platform are given in Table 3.3.

Table 3.3: Properties of the spar platform

Total draft	120 m
Elevation to Platform Top Above SWL	10 m
Depth to Top of Taper Below SWL	4 m
Depth to Bottom of Taper Below SWL	12 m
Platform Diameter Above Taper	6.5 m
Platform Diameter Below Taper Platform	9.4 m
Platform Mass, Including Ballast	7,466,330 kg
CoM Location Below SWL Along Platform Centerline	89.9155 m
Platform Roll Inertia about CoM	4,229,230,000 kg m^2
Platform Pitch Inertia about CoM	4,229,230,000 kg m^2
Platform Yaw Inertia about Platform Centerline	164,230,000 kg m^2
Number of Mooring Lines	3
Angle Between Adjacent Lines	120°
Depth to Anchors Below SWL (Water Depth)	320 m
Depth to Fairleads Below SWL	70 m
Radius to Anchors from Platform Centerline	853.87 m
Radius to Fairleads from Platform Centerline	5.2 m
Unstretched Mooring Line Length	902.2 m
Mooring Line Diameter	0.09 m
Equivalent Mooring Line Mass Density	77.7066 kg/m
Equivalent Mooring Line Weight in Water	698.094 N/m
Equivalent Mooring Line Extensional Stiffness	384,243,000 N
Additional Yaw Spring Stiffness	98,340,000 nm/rad

3.2.1. Static Equilibrium

After the model geometry is defined by the properties from OC3 Phase 4, the model has meshed in grids. Then, the first step in numerical modeling is the investigation of the structure in the static equilibrium case. The combined weight of the turbine and the platform must achieve static buoyancy. The structure is simulated in the time domain under no environmental loading (no wind, or wave) and in still water. Effectively, the only forces present in this case are the gravitational force and the

opposing buoyant force. The structure motion in the time domain simulation is averaged with time and as expected the resulting motion of the structure is near zero for all six degrees of freedom. Static equilibrium results are given in Table 3.4.

Table 3.4: LC 1.3, Static equilibrium results

Surge (m)	Sway (m)	Heave (m)	Roll (°)	Pitch (°)	Yaw (°)
-2.4003e-05	-7.6464e-07	0.0247	2.4980e-07	1.0008e-06	-1.0674e-04

Table 3.4 shows that responses are very close to zero and the model is stable under a static equilibrium case.

3.2.2. Natural Frequencies

The second step of modeling is the investigation of the natural frequencies of the structure. The natural frequencies are obtained for six DOFs and the obtained results are compared with the OC3 participants' results. Natural frequencies for the AQWA model are given in Table 3.5 and a comparison of the natural frequencies with the other participants is provided in Figure 3.2.

Table 3.5: AQWA model natural frequencies (Hz)

Surge-x	Sway-y	Heave-z	Roll-Rx	Pitch-Ry	Yaw-Rz
0.008	0.008	0.0321	0.0341	0.0341	0.0419

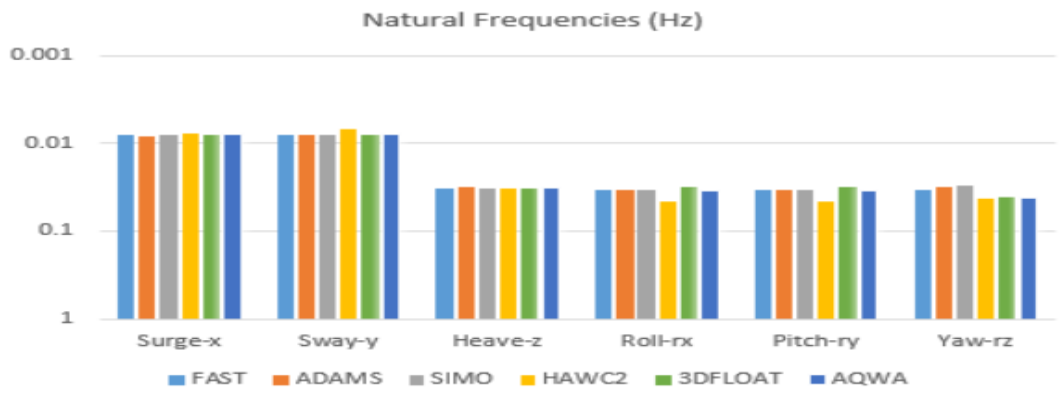

Figure 3.2: LC 1.2, Comparison of the natural frequencies in six DOFs

Figure 3.2 shows that the natural frequencies of the AQWA model are in agreement with the OC3 models' results.

3.2.3. Free Decay Tests

In the third step of the modeling process, LC 1.4 is applied and free decay tests are simulated for the platform at surge, heave, and pitch. In free decay tests, the structure is displaced or rotated from its original position for each degree of freedom, then, the structure response is calculated in the time domain until it reaches the rest meaning that all the forces and moments acting on it are in equilibrium, at its origin position. The calculated responses are given in Figure 3.3 and they are compared with the OC3 results as given in Figure 3.4. Figure 3.3 shows single and coupled responses due to the free decay tests in the surge, heave, pitch degrees of freedom. For example, while the top left plot in Figure 3.3 shows surge response in surge free decay test, the middle and the right plots show the coupled heave and pitch responses under surge free decay test, respectively.

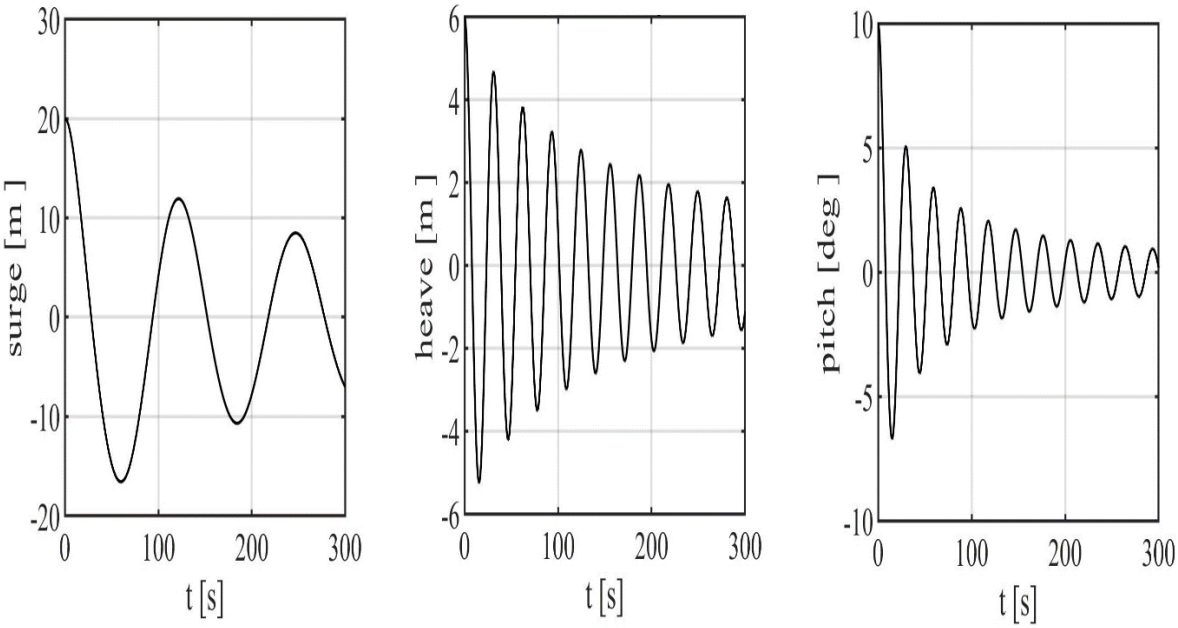

Figure 3.3: LC 1.4 free decay test results in surge, heave, pitch (AQWA)

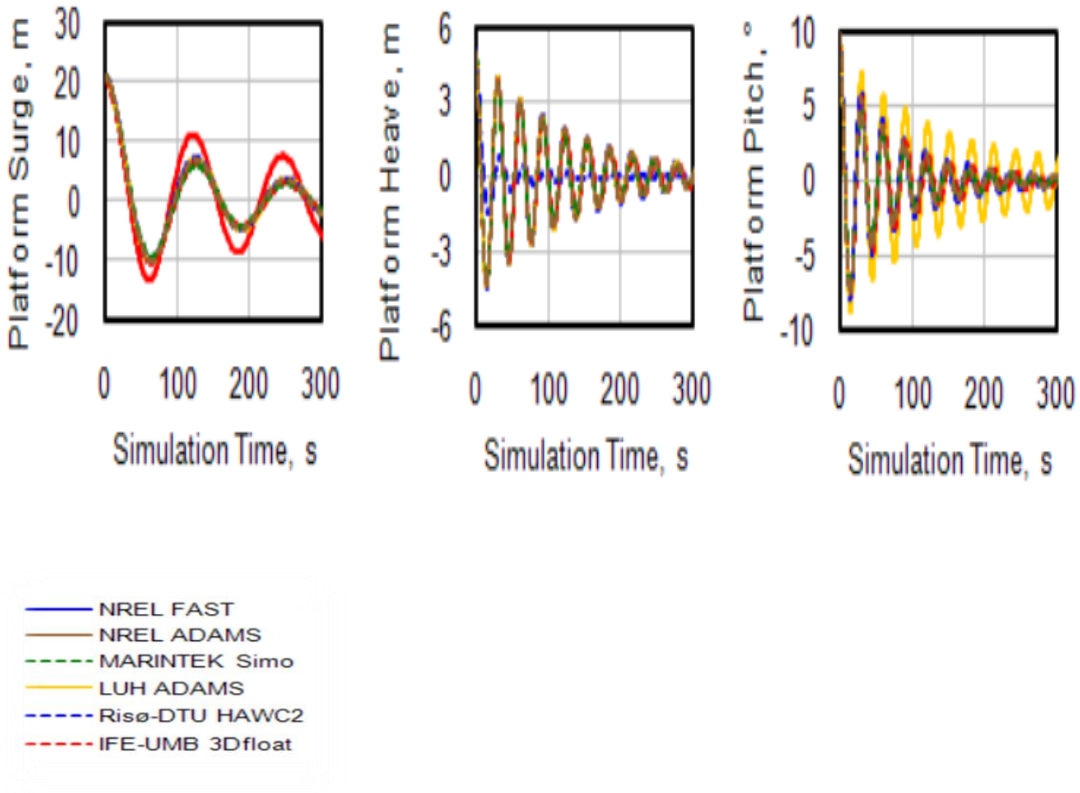

Figure 3.4: LC 1.4 free decay test results in the surge, heave, pitch (OC3)
(source: Jonkman and Musial 2010)

Figure 3.4 shows that the calculated response results of the current model fit the results of other participant's free decay tests.

3.2.4. Hydrodynamic Response with Regular Waves

The next step of the modeling is the investigation of the time-domain response of the spar-type FOWT model under the regular wave load case, LC 4.1. The wave height, H, is 6m, and the wave period, T, is 10 sec. in the regular wave case applied in OC3. The wave incident angle is zero degrees showing the positive x-direction. Under that load case, the surge, heave, and pitch degrees of freedom are taken into consideration in the analysis since they are the only ones excited under zero degrees wave incidence. The dynamic behavior of the structure is investigated under LC 4.1, time histories of the surge and heave displacements, pitch rotation, and seaward cable

tension are simulated and compared with OC3 results.AQWA model time responses are given in Figure 3.5, and OC3 results are given in Figure 3.6 for comparison.

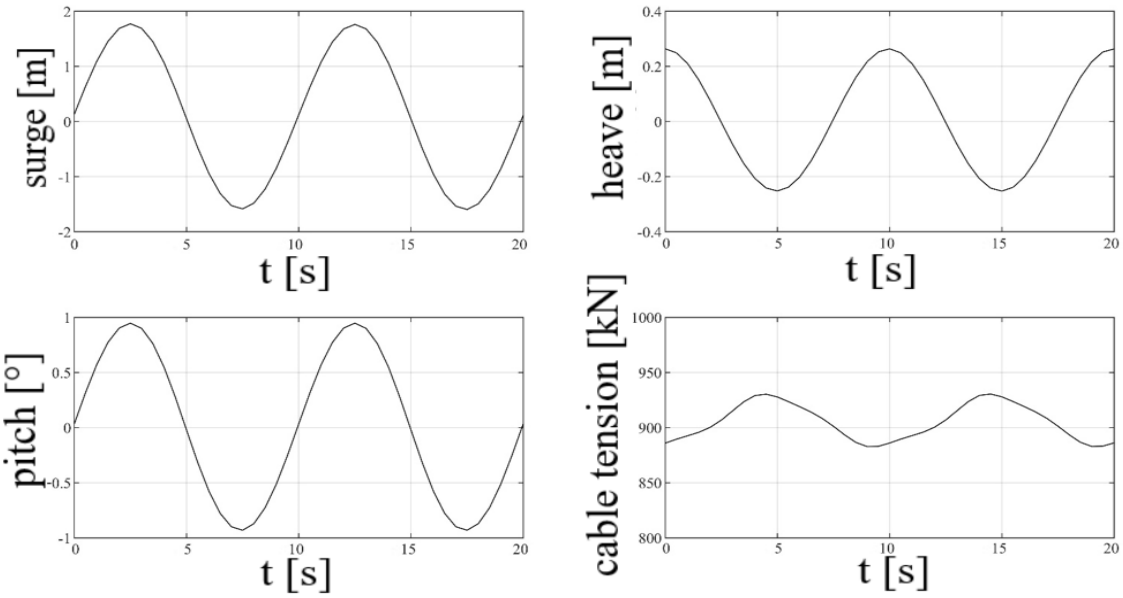

Figure 3.5: LC 4.1 time-domain response analysis results for AQWA model

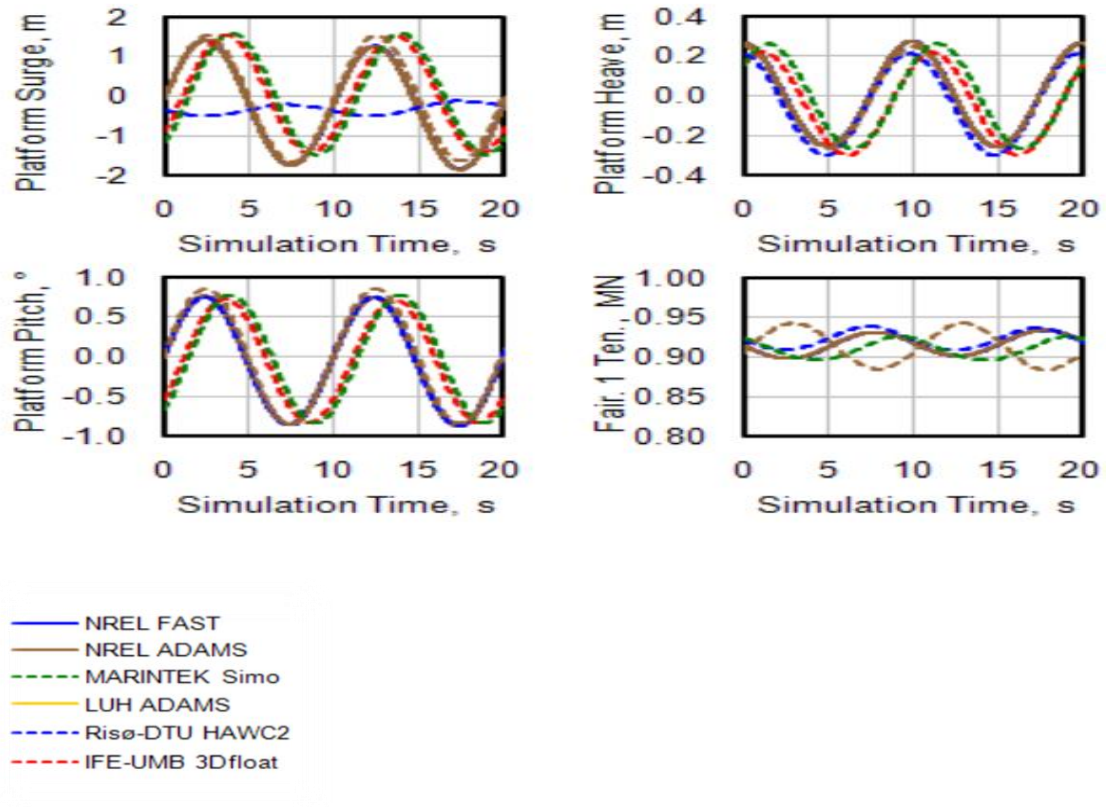

Figure 3.6:: LC 4.1 time-domain response analysis results for OC3 participants (source: Jonkman and Musial 2010)

Figure 3.5 indicates that the surge, heave, pitch responses are in agreement with OC3 results in Figure 3.6 as well as fairlead tension responses. HAWC2 model's discrepancy in the surge is attributed to an error in the output parameter as mentioned in Jonkman and Musial (2010).

3.2.5. Hydrodynamic Response with Irregular Waves

The frequency-domain response of the structure is investigated in the last step of the numerical modeling. Irregular wave parameters are given as input to AQWA. According to LC 4.2, the significant wave height is $H_s = 6\,m$, the peak period is, $T_p = 10\,s$, and the irregular wave series are generated using the JONSWAP spectrum. The wave incident angle is zero degrees showing the positive x-direction, The wave load under zero degree incidence excites the model in the surge, pitch, heave degrees of freedom, and tension forces occur on mooring lines, same as LC 4.1. Platform responses in the relevant DOFs are shown as using energy spectra in the frequency domain. The results for the AQWA model are given in Figure 3.7 and the results of OC3 participants are given in Figure 3.8, on a logarithmic scale.

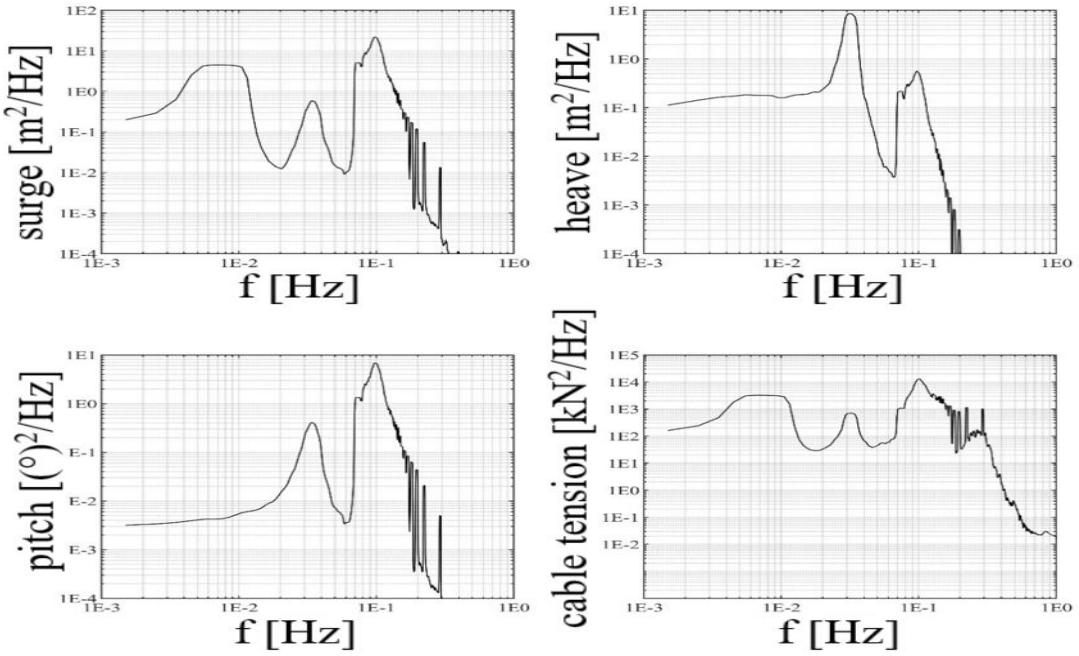

Figure 3.7: LC 4.2 frequency domain response analysis results for AQWA model

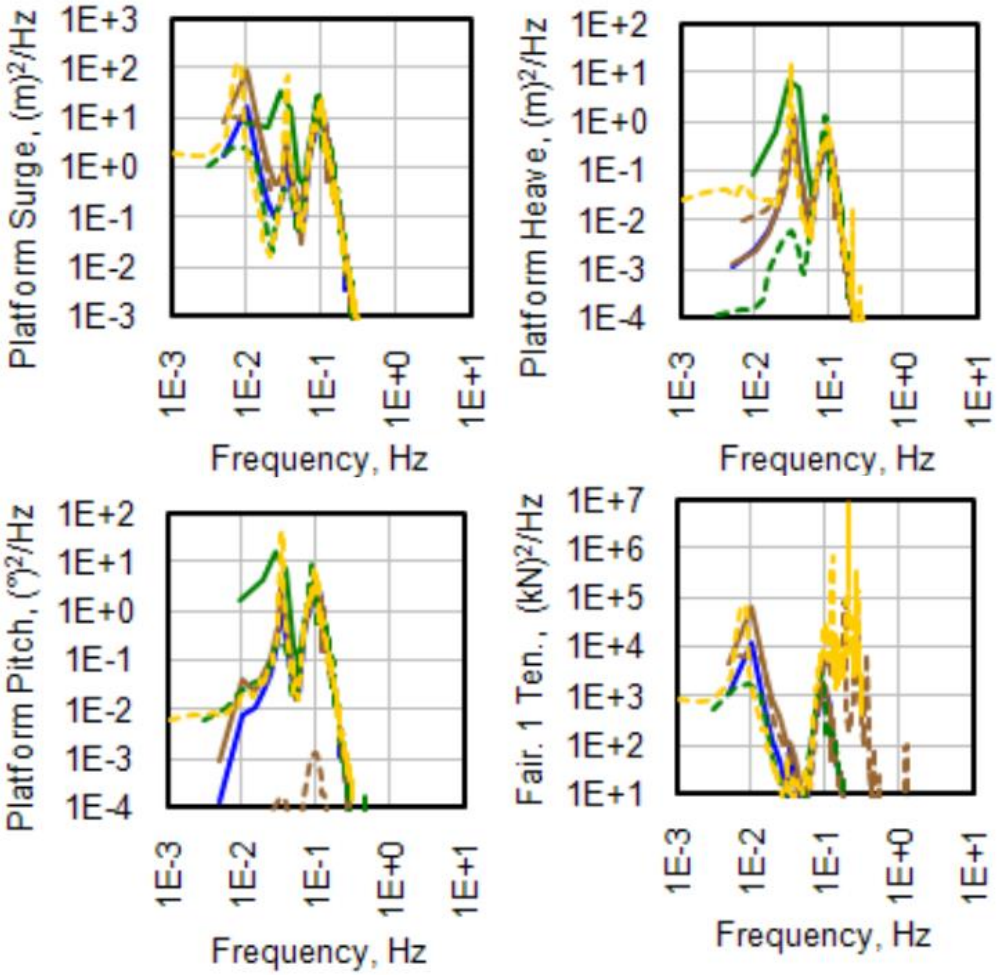

Figure 3.8: LC 4.2 frequency domain response analysis results for OC3 participants (source: Jonkman and Musial 2010)

A comparison between Figure 3.7 and Figure 3.8 indicates that the AQWA model agrees with the other participants' models in all degrees of freedom. As expected, the total energy of the system response is mostly concentrated on 0.1Hz, which is the peak frequency for LC 4.2, and other peaks observed in low frequency are due to structure natural frequencies. It should be emphasized that the system frequency domain response in heave shows a sharper peak in structure's natural frequency than the peak period of the irregular wave, in both figures, leading to the conclusion that in heave DOF, the spar-type FOWT model is mostly undisturbed by wave loads. There are some discrepancies in the magnitudes of spectral estimations for all models. These are attributed to the differences in frequency sampling, which affects the spectral shape.

CHAPTER 4

WAVE GENERATION AND ANALYSIS IN THE LABORATORY

4.1. Wave Environment

To conduct physical model experiments, waves should be generated and analyzed in the laboratory. This study is intended to stimulate, generate and analyze different wave conditions in a laboratory environment. To that end, datasets consisting of regular or irregular wave time series are used. Moreover, the frequency spectrum is used to describe irregular waves in the frequency domain.

4.1.1. Regular Waves

Adhering to the linearized Airy wave theory, regular waves are described as the most basic form of a monochromatic wave (a wave with one distinct frequency and wave height). Under the simplifying assumptions that the fluid is irrotational, inviscid, and incompressible, surface profile solution is derived from the Laplace equation for an ideal fluid:

$$\eta = a \cdot \cos(kx - \omega t + \epsilon) \tag{4.1}$$

and;

$$k = \frac{2\pi}{L};\ \ \omega = \frac{2\pi}{T} \tag{4.2}$$

where η denotes water surface profile, a is the wave amplitude and is the half of the wave height, L is the wavelength, T is the wave period, k is the wavenumber, ω is the wave angular frequency, t is the time, x is the cartesian coordinate in the horizontal axis, and ϵ is the phase of the wave. An example of the water surface profile is given in Figure 4.1.

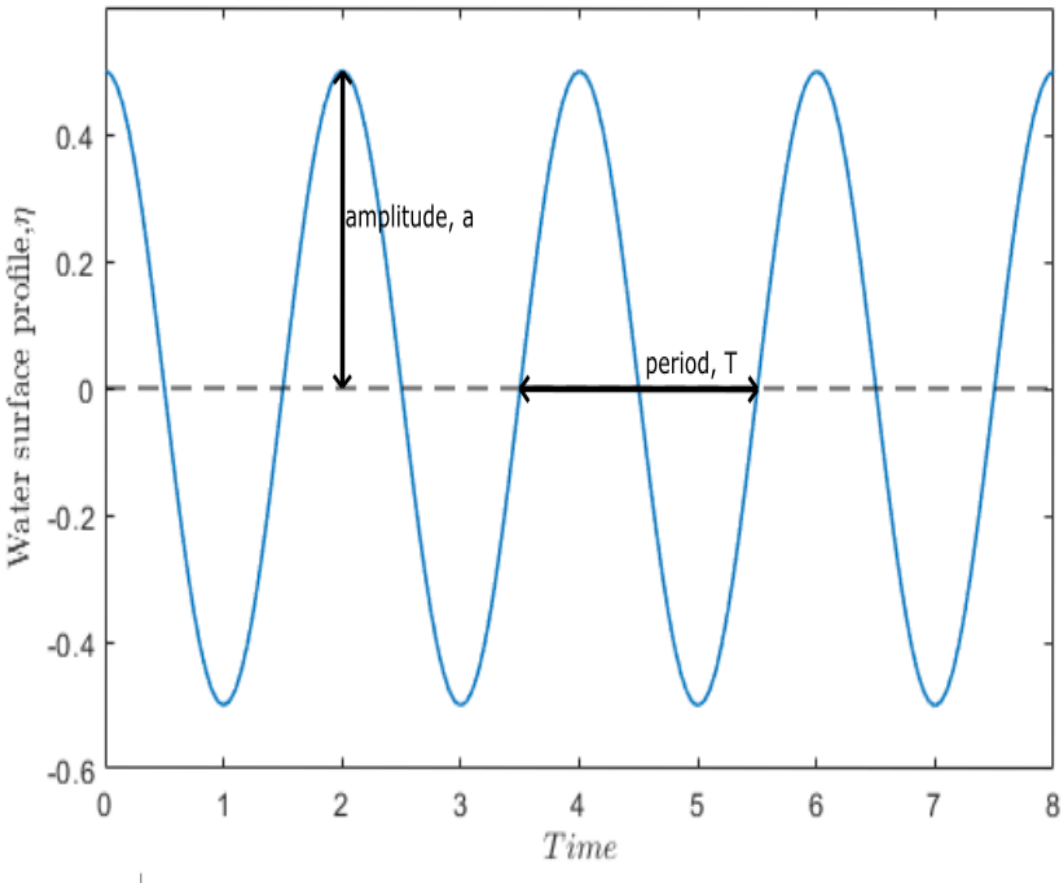

Figure 4.1: Regular wave

The dispersion relation is given as:

$$\omega^2 = gktanh(kh) \tag{4.3}$$

where g represents the gravitational acceleration

A definitive assumption of the Airy wave theory is that wave height is smaller when compared to the water depth and wavelength. Those assumptions linearize the boundary conditions as well as neglecting the higher-order terms, making the solution correct to the first order.

Regular waves are, of course, not encountered in nature. However, their simplicity provides good initial approximations in laboratory experiments as well as numerical studies. Also, regular waves are important when irregular waves are being investigated as they are considered the components of irregular wave series.

4.1.2. Irregular Waves

In laboratory conditions, regular waves can be generated relatively easily. Although being useful in preliminary tests, those waves won't be representative of any real-world simulations. To get a closer approximation to the waves that are observable in nature, irregular waves must be generated.

Irregular waves are often described as the superposition of an infinite number of regular (monochromatic) waves. When the surface profile of a random sea is plotted in the time domain, the resulting form may seem random, however, the same time series can also be investigated in the frequency domain using a Fourier Transform (FT) scheme, which will yield the accumulated wave energies under discrete frequencies, also known as "the spectrum". Over time, numerous spectra are modeled, using the gathered ocean data. An overview of wave spectra is given in the literature review (Chapter 2). Hasselmann (1973) realized fetch limited waves shows characteristically sharper peaks than fully developed PM spectrum, and introduced a "peak enhancement factor" in the definition of the spectrum to better capture this phenomenon. The general expression of wave spectra, given in terms of wave height and period by Goda (1988), is used in this study, which can be used to generate different types of the spectrum such as JONSWAP or Pierson-Moskowitz by changing the input parameters:

$$S(f) = \beta H_s^2 T_p^{1-m} f^{-m} \exp\left[-\frac{m}{n}\left(T_p f\right)^{-\mathrm{n}}\right] \gamma^{\exp\left[-\frac{\left(T_p f-1\right)^2}{2\sigma^2}\right]} \tag{4.4}$$

and;

$$\beta \cong \frac{0.0624\,(1.094 - 0.01915 \ln \gamma)}{0.230 + 0.0336\,\gamma - 0.185(1.9 + \gamma)^{-1}} \tag{4.5}$$

$$\gamma = 1\sim7, \qquad \sigma \cong \begin{cases} 0.07: & f \le f_p, \\ 0.09: & f > f_p. \end{cases} \tag{4.6}$$

where, H_s denotes significant wave height which corresponds to the mean value of 1/3$^{\text{th}}$ of all individual wave heights in the zero-up crossing method, T_p is the peak period in the wave spectrum, γ is the aforementioned peak enhancement factor which can be ranged between 1 to 7 with a typically used mean value of 3.3, f denotes the discrete

frequencies in the spectrum, and f_p is spectral peak frequency which is the multiplicative reciprocal of T_p. When m and n are equal to 5 and 4, respectively, and γ is equal to 1.0, Eq. 4.4 gives the the definition of PM spectrum. The comparison of PM and JONSWAP spectra with γ =3.3 is given in Figure 4.2.

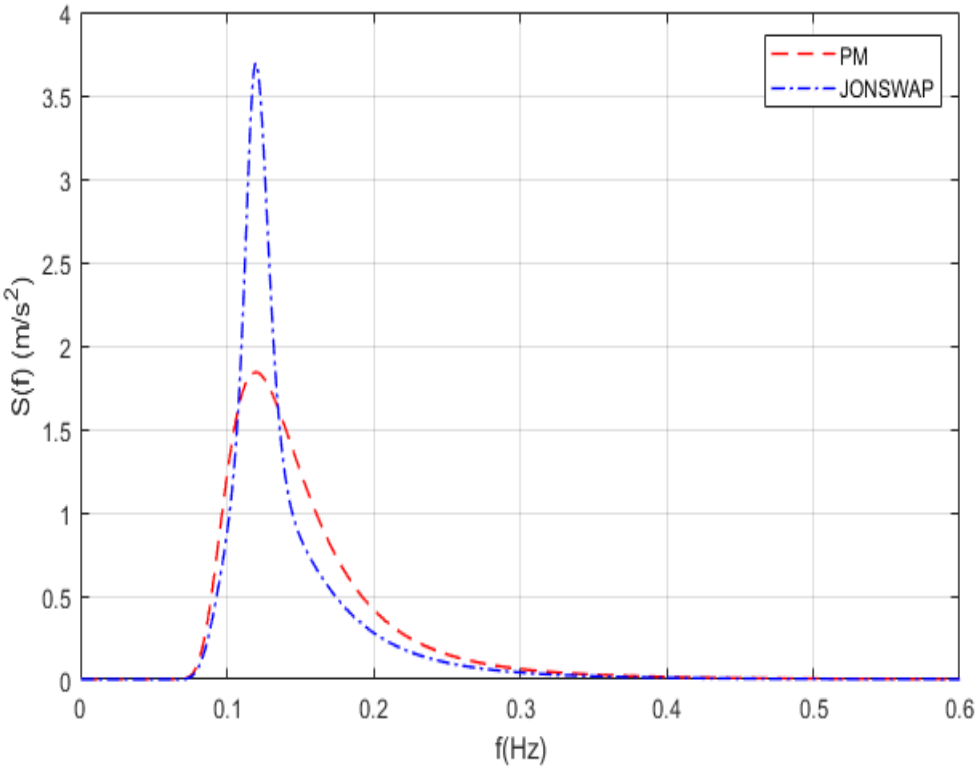

Figure 4.2: A comparison of PM and JONSWAP spectrum with the same wave parameters (Hs=1.5m, Ts=7.6s)

4.2. Analysis Procedures of Wave Datasets

Being able to process the wave data is important to understand the properties of the wave train, and it is also a critical step in the synthesis of random waves. Several methods will be described here used in the analysis of time series of random waves which are either generated theoretically or measured during the tests of laboratory experiments. The procedures to obtain the frequency spectrum from time-domain data and to derive irregular wave properties from created spectra are explained. Being able to process the data in time and frequency domains opens up the possibility to obtain

entirely random wave time series with desired wave characteristics. These procedures also enable the user to make proper validations between theoretical results and experimental ones.

4.2.1. Frequency Domain Analysis

The most basic form of a sine wave, also known as a regular wave, can be described with a trigonometric function consisting of wave amplitude and wave period. However, that function is never going to properly define realistic wave profiles. Fortunately, irregular waves as seen in nature can be idealized as the superposition of an infinite number of regular waves, which brings the possibility to decompose the irregular wave series to its regular wave components. An irregular wave consisting of an infinite regular wave series with many frequencies, amplitudes, and phases can be mathematically described as a time-dependent function:

$$x(t) = \sum_{n=0}^{\infty} a_n \cos(\omega_n t - \epsilon_n) \tag{4.7}$$

where a_n denotes wave amplitude, ω_n angular wave frequency, and ϵ_n the phase of each wave in the time domain.

Using the Eulerian identity:

$$e^{i\theta} = cos\theta + isin\theta \tag{4.8}$$

Fourier transform in the complex form can be defined:

$$X(\omega) = A(\omega) - iB(\omega) \tag{4.9}$$

and,

$$\begin{aligned} A(\omega) &= \frac{1}{2\pi}\int_{-\infty}^{\infty} x(t) cos\omega t dt \\ B(\omega) &= \frac{1}{2\pi}\int_{-\infty}^{\infty} x(t) sin\omega t dt \end{aligned} \tag{4.10}$$

where $A(\omega)$ and $B(\omega)$ here are two continuous components of the Fourier transform. Substituting Eq. (4.10) into Eq. (4.9) and using the Eulerian identity in Eq. (4.8) yields:

$$X(\omega) = \frac{1}{2\pi}\int_{-\infty}^{\infty} x(t)(cos\omega t - isin\omega t)dt = \frac{1}{2\pi}\int_{-\infty}^{\infty} x(t)e^{-i\omega t}dt \quad (4.11)$$

Eq. (4.11) is the complex representation of the Fourier transform and can be used effectively to describe the time-domain function in the frequency domain. Fourier transforms can also be used to convert functions in the frequency domain to time domain representations using the form termed as 'inverse Fourier transform'. Inverse Fourier transform is described in the complex form as:

$$x(t) = \int_{-\infty}^{\infty} X(\omega)e^{i\omega t}d\omega \quad (4.12)$$

Using Fourier transform in a procedure known as 'Fast Fourier Transform' 'FFT' allows the user to calculate the discrete Fourier transform of a periodic process with N discrete data points, resulting spectral coefficients are in the complex form of:

$$X_n = a - ib \qquad ; n = 0,1, \dots, (N-1) \quad (4.13)$$

At the discrete frequency points in which a and b are the Fourier components and the magnitude of the spectral amplitudes can be calculated as:

$$S_n = X_n \cdot X_n^* \qquad ; n = 0,1, \dots, (N-1) \quad (4.14)$$

where X_n^* is the complex conjugate of the spectral coefficients, and S_n is the spectral amplitude, also known as 'magnitude', at n'th discrete frequency. Frequency sampling in an FFT scheme is directly dependent on the time step of the discrete-time series:

$$\begin{matrix} f_n = n \cdot df \\ df = 1/N\Delta t \end{matrix} \qquad ; n = 0,1, \dots, (N-1) \quad (4.15)$$

where Δt denotes the time step, df is the sampling frequency, and f_n the discrete frequency at the n'th point in the series. The frequency spectrum is created when the resulting spectral amplitudes are plotted against the discrete frequencies. Since the area under the energy spectrum represents the total wave energy, when the energy spectrum is plotted for wave measurement taken at discrete time steps, the resulting plot will give ideas about the frequencies where the wave energies are the most dominant. If FFT is applied and the spectrum is plotted for a regular wave, the spectrum will show one peak as there is just one wave frequency and all wave energy is concentrated there, but for an irregular wave train, the frequency spectrum will show the distribution of different energy levels on different discrete frequencies. Time series and frequency spectrum

examples of a bichromatic wave (two regular waves with different frequencies) and an irregular wave are given in Figure 4.3

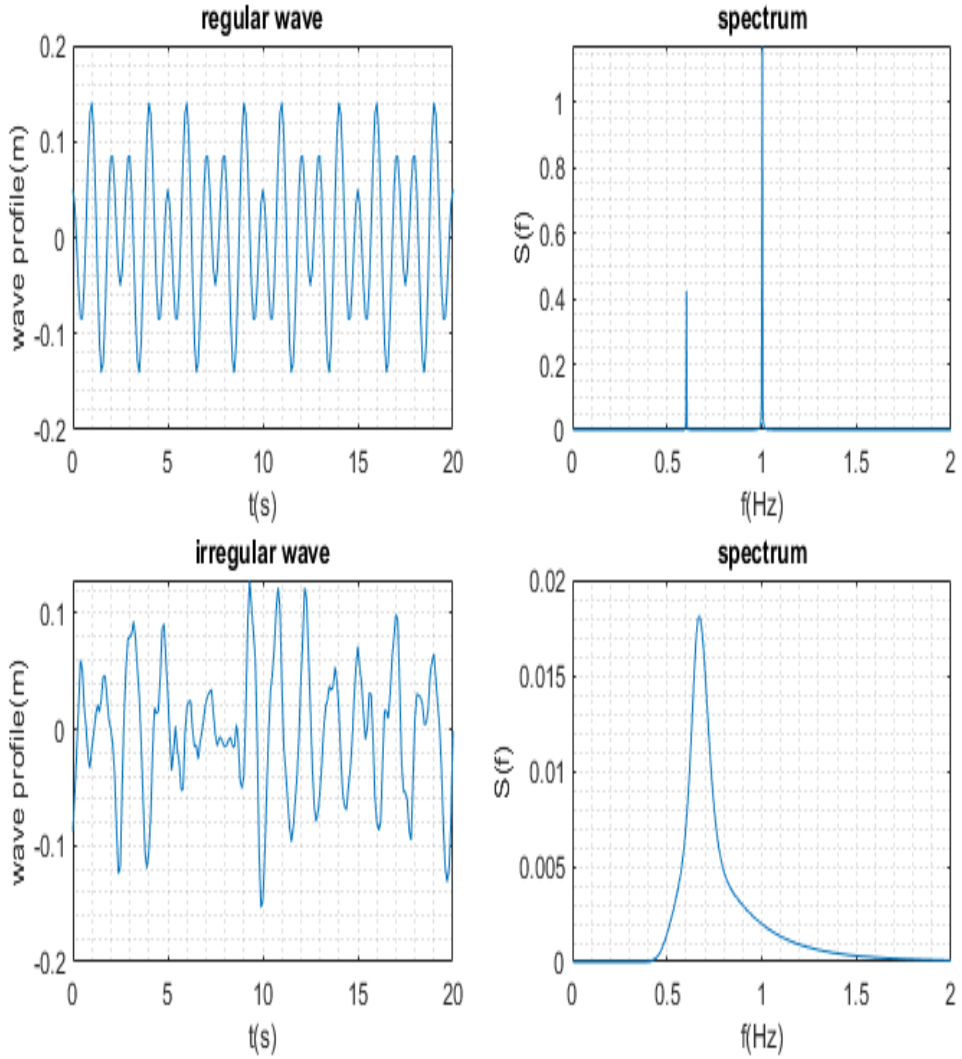

Figure 4.3: Time series (left) and spectra (right) of a bichromatic wave (up) and an irregular wave (down)

Many programming languages offer built-in methods for FFT calculations. Details of the FFT technique can be found in Newland (2012).

4.2.2. Spectral moments

It is also possible to extract the wave characteristics from the spectral description of the sea waves. Representative wave heights and periods can be derived from the wave energy spectrum. The concept of spectral moments is used to that end, and its definition for the nth moment of the spectrum is given as (Mackay 2012):

$$m_n = \int_0^\infty f^n S(f) df \tag{4.16}$$

here, m_n describes the nth moment of the spectrum, f is frequency and $S(f)$ is the value of the energy spectrum function at the frequency, f.

It is mentioned earlier that the area under the energy spectrum represents the total wave energy. The area under the spectrum function can be found by integrating it over the frequency range. In other words, total wave energy should correspond to m_0, the zeroth moment of the spectrum. A practical approach to calculate the area is using the so-called "trapezoid rule". It is a simple and efficient procedure and many programming languages offer libraries with built-in functions that include this procedure.

Other relationships between spectral moments and wave parameters are given as:

$$H_{m0} \approx 4.004\sqrt{m_0} \tag{4.17}$$

$$\bar{T} = \sqrt{\frac{m_0}{m_2}} \tag{4.18}$$

$$T_p = \frac{1}{f_p} \tag{4.19}$$

the frequency corresponding to the peak point of the spectrum function is termed peak frequency, f_p and reciprocal of f_p yield the peak period, T_p.

4.2.3. Time Domain Analysis

For the time domain analysis, the zero-up crossing method is widely used to determine the individual waves in irregular wave time series. Initially, the mean water level is determined by averaging the whole water surface profile and defined as the zero lines or still water level. Then, starting from the beginning of the wave record, points are searched where the surface profile crosses the zero line upward. The surface profile

between two consecutive zero-up crossing points is taken as one individual wave. The difference between the maximum and the minimum of water surface elevation in each wave is noted as the individual wave height. The duration between the starting and ending points of each wave is noted as the corresponding individual wave period. Using zero-up crossing methods all of the individual wave heights and their corresponding wave periods are calculated.

After the determination of the individual waves, some characteristic waves should be defined for an irregular wave environment. To determine the characteristic waves of the time series, individual waves calculated by the zero-up crossing method are sorted in descending order according to the wave heights. While the wave height of the highest wave in the wave record is denoted H_{max} , the period corresponding to H_{max} is named T_{max}. Mean wave heights and periods are calculated using all waves in the wave record, and they are denoted $\bar{H}$ and $\bar{T}$, respectively. The highest one-third wave (33%), also known as the significant wave is defined as the mean values of wave heights and periods of the highest one-third of the individual waves in the wave record. They are denoted as $H_{1/3}$ and $T_{1/3}$ or H_s and T_s, respectively. Significant wave heights and periods are important because they are the most frequently used characteristic waves in the various coastal engineering activities like the stability of the rubble mound. In this study, the zero-up crossing method is used in the validation process of the synthesis of random waves and the calculation of measured wave properties of the waves generated in the laboratory experiments.

4.3. Preparation of the Wave Generator Signal

In this study, the deterministic spectral amplitude method is used in the random generation of irregular wave time series. In this section, the "Deterministic spectral amplitude method (DSA)" is explained and an example is provided as well as the validation used in the process. Next, the wavemaker theory is given and solutions are provided to the first and second-order for regular and irregular waves. A flow chart describing the steps in the generation of waves for the laboratory experiments is provided in Figure 4.4.

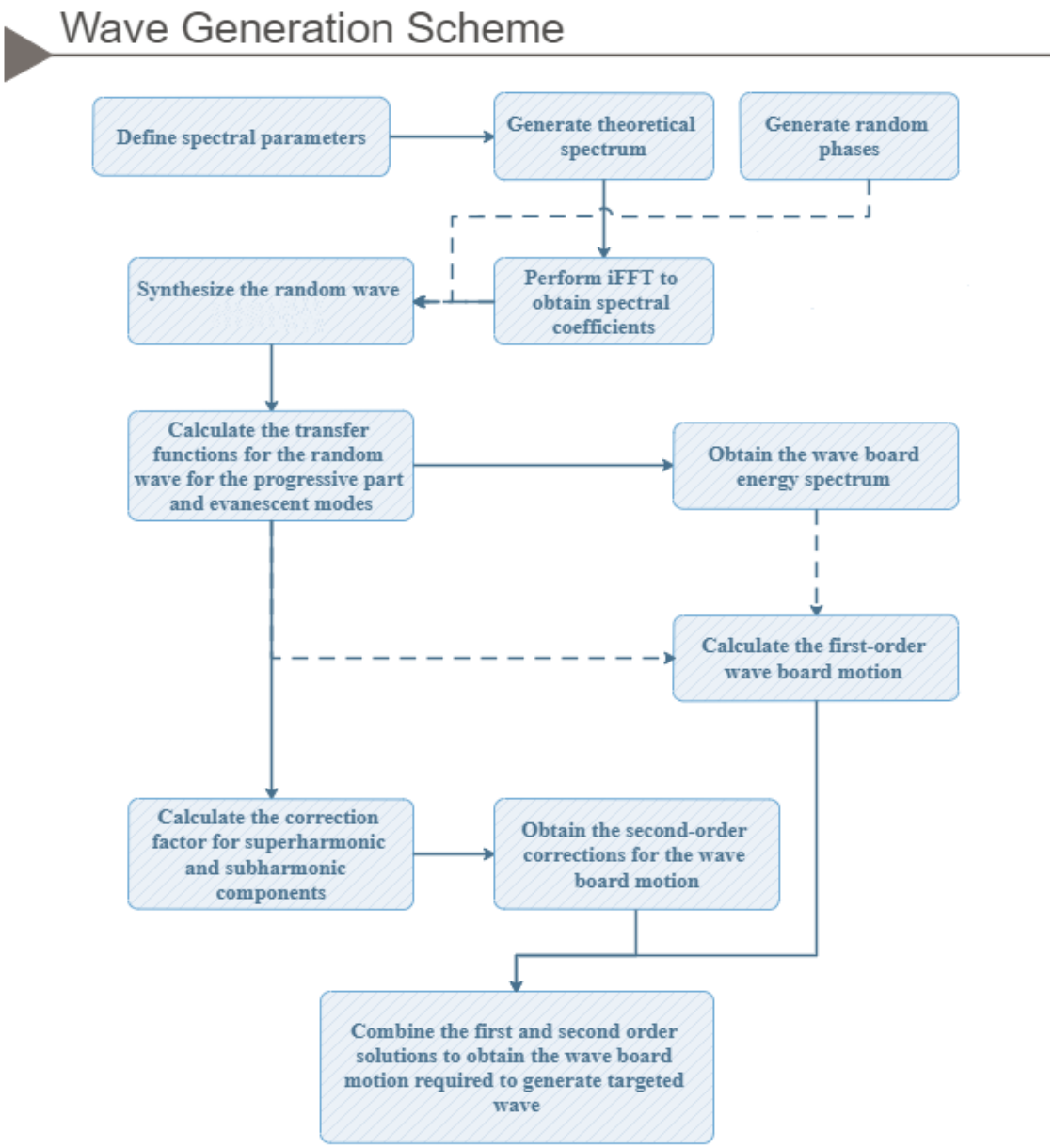

Figure 4.4: Flow chart describing the steps involving wave generation

4.3.1. Synthesis of the Irregular Wave Series

To synthesize irregular waves, the Deterministic Spectral Amplitude (DSA) method (Tuah and Hudspeth,1982) is used in this study. This method allows the synthesis of irregular wave time series that have the spectral properties of a targeted spectrum. The premise of the adopted wave synthesis scheme is that as the frequency

spectrum can be obtained from wave time series using FFT, inversely, time series can be generated from any given spectra. Moreover, time-domain representations of any wave consist of two elements; amplitude and phase, and yet, due to the nature of Fourier transformation, phase knowledge of the series is lost after the application of FFT. Therefore, to synthesize a new wave time series, the DSA model proposes to use randomly generated phases to be included in the inverse Fast Fourier Transform (iFFT). This method effectively makes it possible to generate an infinite number of irregular wave series that all adhere to the targeted spectral form. In the application of the method the followed steps are explained below;

1 – Using significant wave height, and peak spectral frequency as inputs, a target spectrum is formed using Eq. (4.4)

2 – With a random number generator, a phase sequence of zero mean and unit variance is generated in the range between 0 to 2π

3 – Fourier coefficients are calculated using the relation given below:

$$A_n = N\left(\frac{S(f_n)df}{2}\right)^{0.5} e^{i\theta_n} \qquad n = 1,2,\dots,N \tag{4.20}$$

where N is the total number of discrete data points, $S(f_n)$is the wave spectral density at nth frequency, df is the frequency sampling rate, θ_n is the nth phase in the randomly generated phase sequence, and A_n denotes the Fourier coefficients.

4 – Fourier coefficients sequence are extended by mirroring A_n series with the complex conjugate of A_n

5 – Inverse FFT (iFFT) is applied to the Fourier coefficients, which, in the end, generates $2N$ number of discrete water surface profile values from N number of discrete wave energy spectrum.

The method is reported to produce realistic water surface profiles for large N Wang and Crouch (1993). Also, to increase efficiency in the FFT scheme, the value of N is always chosen as 2^m.

After synthesizing the random wave series, a two-step validation process is applied by a computer program written in house. First, the wave energy spectrum is re-derived from the synthesized random irregular wave. The re-derived wave spectrum is

compared to the target spectrum. Second, the zero-up crossing is applied to the random wave time series to calculate the characteristic wave height and periods. The same wave properties are also calculated from the spectral moments of the obtained wave energy spectrum, and those are compared to the zero-up crossing results. It is known that the wave height calculated using Eq.(4.17) from the spectrum (H_{m0}) should be close to significant wave height, Hs calculated from the time series by the zero-up crossing method. Furthermore, the relation between the peak period (T_p) and the siginificant wave period (T_s) defined by Mitsuyasu (1970) is checked using the formula given below:

$$T_p = 1.05T_s \tag{4.21}$$

If the comparisons in both steps agree with each other, then it can be concluded that the spectrum function is applied correctly in the program and the generated random irregular wave exhibits the targeted wave characteristics.

An example of irregular wave generation is provided with parameters $T_p = 1.5s$, $H_s = 0.25m$. The frequency spectrum type is JONSWAP with $\gamma = 3.3$. The total number of discrete data points is chosen as, $N = 8192$, and the time step is $\Delta t = 0.01s$. The time series for the water surface profile is given in Figure 4.5.

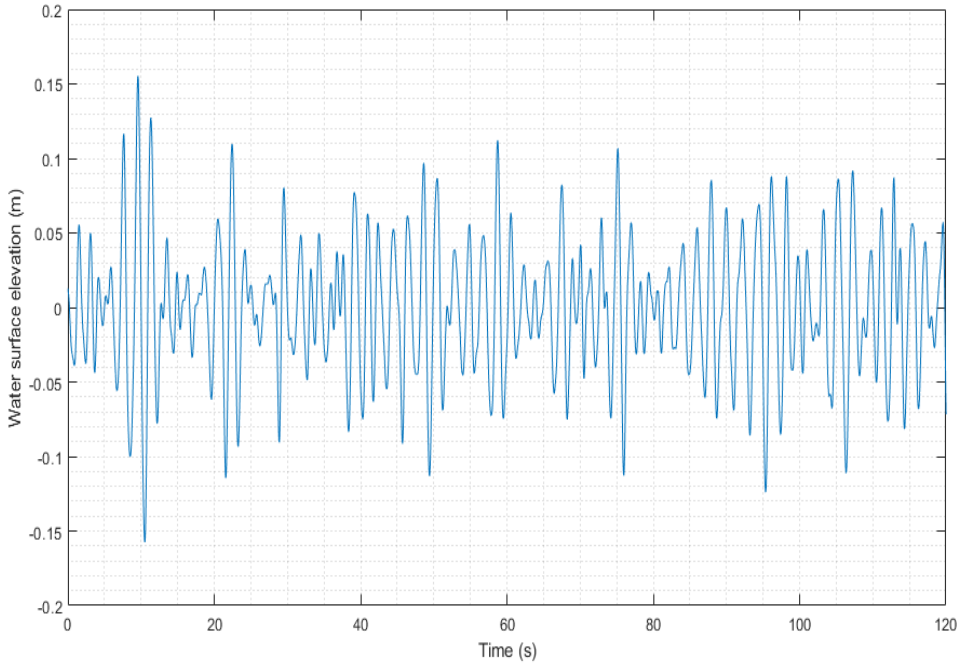

Figure 4.5: Randomly generated irregular wave series

To validate the wave generation scheme, the theoretical target spectrum is compared to the spectrum derived from the irregular wave time series given in Figure 4.6.

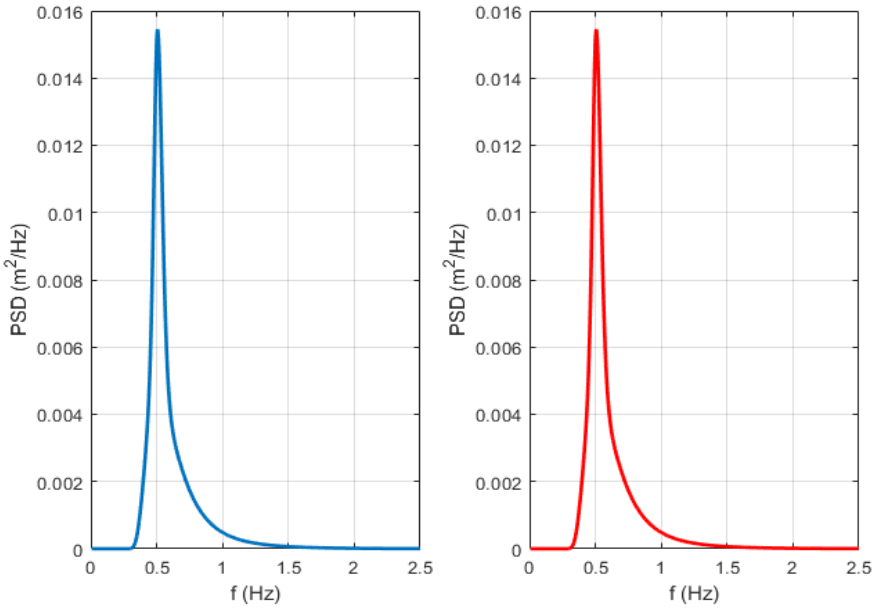

Figure 4.6: Comparison of the theoretical spectrum obtained by Eq.(4.4)(left), and the one obtained from the synthesized irregular waves (right)

As can be seen in Figure 4.6, the spectrum obtained from the synthesized time series and the theoretical spectrum are the same. This verifies that the DSA method is applied correctly in this study. Table 4.1 provides the comparison of the wave properties from both spectral moments and zero-up crossing of the random wave time series. Ratios of the differences between H_s and T_{mean} values are checked and found to be within acceptable parameters that are rough ~5% and ~7% (Goda, 1979; 2000).

Table 4.1: Validation of the wave generation scheme with spectral and statistical parameters

Parameters	Values Derived From Spectral Moments	Statistical Values From Zero-up Crossing
H_s	0.20 m	0.195 m
T_s	1.90 s	1.88 s
T_{mean}	1.55 s	1.54 s

4.3.2. Wave Board Displacement Functions by Wavemaker Theory

The foundation of the theory of wavemakers was led by Havelock (1929), considering the waves as the vertical oscillations of the water surface forced by a planar or cylindrical solid body. The theory was later extended by Biesel (1951), which provided solutions to different types of wave generators such as piston or flap type. Then, the theory has been improved extensively for both regular (Fontanet 1961) and irregular waves (Sand and Mansard, 1986; Schäffer, 1996). A sketch for the generalized wave generator in a two-dimensional wave flume is given in Figure 4.7.

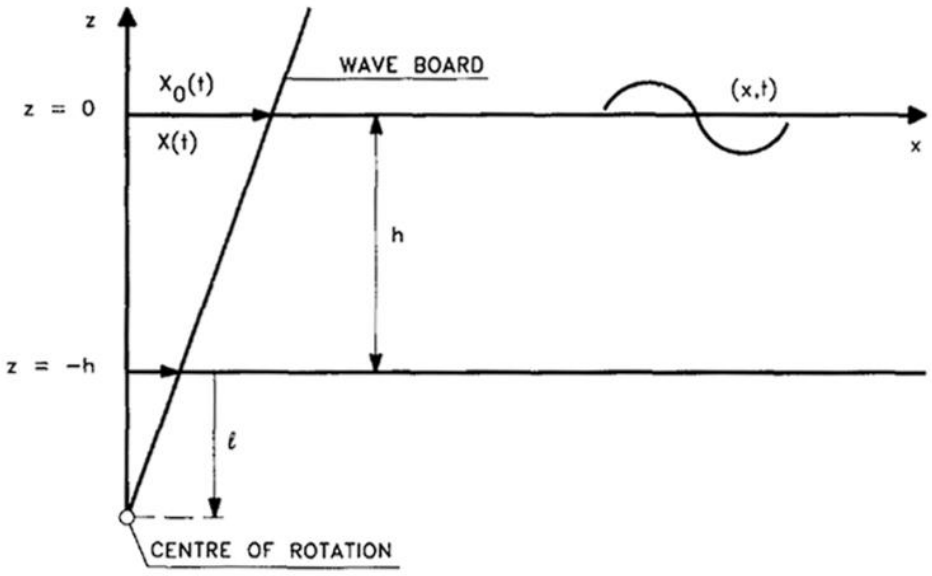

Figure 4.7: A 2-D sketch of the generalized wave generator system
(source: Schäffer 1996)

Wave generators may force the water waves with translational or rotational motion, or a combination of the two. Assumptions are made that the fluid is incompressible, inviscid, and irrotational, surface tension is neglected, the bed of the flume is horizontal, flat, and impermeable. Also, the condition at the wave board is that the velocity gradient normal to the surface of the wave board is equal to the velocity of the fluid in the same direction. Laplace equation in two dimensions is used in a Cartesian coordinate system and is assumed to describe the motion of the fluid in the

wave flume. Following boundary conditions and boundary value problems are given below, adhering to the notation used by Barthel et al. (1983) and (Schäffer 1996):

Let $\phi = \phi(x, z, t)$ define the velocity potential and $u = \phi_x, v = \phi_z$

Laplace equation:

$$\Delta\phi = 0 \qquad everywhere \tag{4.22}$$

Dynamic free surface condition:

$$\phi_t + \frac{1}{2}(\phi_x^2 + \phi_z^2) + g\eta = 0 \qquad for\ z = \eta \tag{4.23}$$

Kinematic free surface condition:

$$\eta_t + \phi_x\eta_x - \phi_z = 0 \qquad for\ z = \eta \tag{4.24}$$

Impermeable bottom condition:

$$\phi_z = 0 \qquad for\ z = -h \tag{4.25}$$

Wave board condition:

$$\phi_x = \left(1 + \frac{z}{h+l}\right) X_{o_t} \qquad for\ x = X(z,t) \tag{4.26}$$

where $\eta = \eta(x,t)$ is the water surface elevation, $g, h, and\ t$ are the gravitational acceleration, water depth, and time, respectively. h, l, and z are shown in Figure 4.7.

The wave board position is given as:

$$X(z,t) = f(z)\, X_0(t) \tag{4.27}$$

where $f(z)$ is a function that describes the type of wavemaker:

$$f(z) = \begin{cases} 1 + \dfrac{z}{h+l} & for -(h-d) \le z \le 0 \\ 0 & for -h \le z < -(h-d) \end{cases} \tag{4.28}$$

where $z = -(h+l)$ is used to describe the center of rotation and $d \geq 0$ is the elevation of the hinge over the bottom. For a piston-type wavemaker, the center of rotation has the limit $l \to \infty$ and $d = 0$, making the second case in (4.28) inapplicable.

The solution scheme for this problem requires the Taylor series expansion to be applied to the Eqs. (4.23) - (4.26), which will yield boundary conditions at $x = 0$ and $z = 0$. Next, using the perturbation theory, the terms ϕ, η, and X_0 are rewritten as perturbation series:

$$\phi = \epsilon\phi^{(1)} + \epsilon^2\phi^{(2)} \tag{4.29}$$

$$\eta = \epsilon\eta^{(1)} + \epsilon^2\eta^{(2)} \tag{4.30}$$

$$X_0 = \epsilon {X_0}^{(1)} + \epsilon^2 {X_0}^{(2)} \tag{4.31}$$

where ϵ is the small ordering parameter that is proportional to wave steepness (Flick and Guza 1980). The solution procedure yields the resulting boundary value problems:

$$\phi_{tt} + g\phi_z = R \qquad for\ z = 0 \tag{4.32}$$

$$\phi_x = Q \qquad for\ x = 0 \tag{4.33}$$

$$\eta = \frac{1}{g}(\phi_t + P) \qquad for\ z = 0 \tag{4.34}$$

$$\phi_z = 0 \qquad for\ z = -h \tag{4.35}$$

for the first-order problem R, Q and P becomes for $(\phi, \eta) = (\phi^{(1)}, \eta^{(1)})$:

$$R^{(1)} = 0 \tag{4.36}$$

$$Q^{(1)} = f(z)X_{0t}^{(1)} \tag{4.37}$$

$$P^{(1)} = 0 \tag{4.38}$$

and for the second-order problem R, Q and P becomes for $(\phi, \eta) = (\phi^{(2)}, \eta^{(2)})$:

$$R^{(2)} = -\left\{\left(\phi_x^{(1)^2} + \phi_z^{(1)^2}\right)_t + \eta^{(1)}\left(\phi_{tt}^{(1)} + g\phi_z^{(1)}\right)_z\right\} \tag{4.39}$$

$$Q^{(2)} = -X_0^{(1)}\left\{f(z)\phi_{xx}^{(1)} - \frac{1}{h+l}\phi_z^{(1)}\right\} + f(z){X_0}_t^{(2)} \tag{4.40}$$

$$P^{(2)} = \frac{1}{2}\left(\phi_x^{(1)^2} + \phi_z^{(1)^2}\right) + \eta^{(1)}\phi_{zt}^{(1)} \tag{4.41}$$

4.3.2.1. Spurious Harmonic Waves

Before proceeding to the solution of the wavemaker problem, it is worth mentioning the spurious harmonic waves. In the solution of the wavemaker problem to the second-order, due to the linearity of the boundary value problems Barthel et al. (1983) rewrote $\phi^{(2)}$ as the superposition of three components:

$$\phi^{(2)} = \phi^{(21)} + \phi^{(22)} + \phi^{(23)} \tag{4.42}$$

where the $\phi^{(21)}$ gives the second-order bound long waves and the solution of it describes the progressive waves. Boundary conditions that $\phi^{(22)}$ have to satisfy contain

terms that correspond to spurious waves which should not be on a natural wave train. One term that occurs due to the local disturbances is termed as “local disturbance waves”, another free long wave that arose due to the wave board leaving its mean position is termed “displacement wave”, and the third free wave which is generated due to the negative component of the progressive wave which represents the orbital velocity reflecting off the wave board surface is termed the “parasitic long wave”. Therefore, to eliminate those spurious long waves $\phi^{(23)}$ must have the condition:

$$\phi^{(22)} + \phi^{(23)} = 0 \tag{4.43}$$

in other words, to eliminate the spurious-free waves, the second-order wavemaker solution must determine $X_0^{(2)}(t)$ so that $\eta_0^{(23)}$ should satisfy:

$$\eta_0^{(22)} + \eta_0^{(23)} = 0 \tag{4.44}$$

In that pattern, the boundary value problems in Eq. (4.39)-(4.41) become:

for $(\phi,\ \eta) = \left(\phi^{(21)}, \eta^{(21)}\right)$:

$$R^{(21)} = -\left\{\left({\phi_x^{(1)}}^2 + {\phi_z^{(1)}}^2\right)_t + \eta^{(1)}\left(\phi_{tt}^{(1)} + g\phi_z^{(1)}\right)_z\right\} \tag{4.45}$$

$$Q^{(21)} = arbitrary \tag{4.46}$$

$$P^{(21)} = \frac{1}{2}\left({\phi_x^{(1)}}^2 + {\phi_z^{(1)}}^2\right) + \eta^{(1)}\phi_{zt}^{(1)} \tag{4.47}$$

for $(\phi,\ \eta) = \left(\phi^{(22)}, \eta^{(22)}\right)$:

$$R^{(22)} = 0 \tag{4.48}$$

$$Q^{(22)} = \begin{cases} -X_0^{(1)}\left\{f(z)\phi_{xx}^{(1)} - \dfrac{1}{h+l}\phi_z^{(1)}\right\} - \phi_x^{(21)},\ for - (h-d) \le z \le 0 \\ \phi_x^{(21)},\ \ for - h \le z < -(h-d) \end{cases} \tag{4.49}$$

$$P^{(22)} = 0 \tag{4.50}$$

and for $(\phi,\ \eta) = \left(\phi^{(23)}, \eta^{(23)}\right)$:

$$R^{(23)} = 0 \tag{4.51}$$

$$Q^{(23)} = f(z)X_{0t}^{(2)} \tag{4.52}$$

$$P^{(23)} = 0 \tag{4.53}$$

In the solution provided by Barthel et al. (1983) only the difference frequencies are deemed of interest because they produce long wave terms. However, a later study by Sand and Mansard (1986) showed that summation frequencies also have free harmonic

contributions that must be dealt with, and also, a wavemaker theory that includes summation frequencies produces more realistic waves with sharper crests and flatter throughs. Sand and Mansard (1986) also generalized the terms given by Barthel et al. (1983) to "subharmonics" for difference frequency terms and "superharmonics" for summation frequency terms.

4.3.2.2. Generation of Regular Waves

Due to the simpler theoretical nature of regular waves, wave board solution in the wavemaker theory was established firstly. The solution was provided by considering the boundary value problems in Eq. (4.32) to Eq.(4.35), then applying the separation of variables technique to separate the Laplace equation into ordinary differential equations with known solutions. Summation of the solutions where the separation constant is real $k_1^2 > 0$, $k_2 = 0$, and imaginary $k_3^2 < 0$, gives the solution to the general velocity potential function (Flick and Guza 1980):

$$\phi^{(1)}(x,z,t) = A\cosh[k_1(h+z)]\sin(k_1 x - \omega t) + \cos\omega t \sum_{n=1}^{\infty} C_n e^{-k_{3_n}x}\cos[k_{3_n}(z+h)] \tag{4.54}$$

and,

$$A = \frac{\omega S_0 \int_{-h}^{0} f(z)\cosh[k_1(h+z)]dz}{2k_1 \int_{-h}^{0}\cosh^2[k_1(h+z)]dz} \tag{4.55}$$

$$C_n = \frac{\omega S_0 \int_{-h}^{0} f(z)\cos\left[k_{3_n}(h+z)\right]dz}{2k_{3_n} \int_{-h}^{0}\cos^2[k_{3_n}(h+z)]dz} \tag{4.56}$$

where S_0 denotes the wave board stroke at $z = 0$ and:

$$X_0^{(1)} = \frac{S_0}{2}\sin\omega t \tag{4.57}$$

water surface elevation in the wave flume is found as:

$$\eta^{(1)}(x,t) = \frac{\omega A}{g}\cosh\,(\mathrm{k}_1 h)\cos(k_{1x} - \omega t) + \sin(\omega t)\sum_{n=1}^{\infty}\frac{\omega C_n}{g}e^{-k_{3_n}x}\cos(k_{3_n}h) \tag{4.58}$$

for the solution away from the wave board, summation terms drop:

$$\eta^{(1)}(x,t) = H\cos(k_1 x - \omega t) \tag{4.59}$$

where H is the wave height. After the Eqs. (4.58) and (4.59) are evaluated together, the basic wavemaker relationship is formed:

$$H = \frac{2\omega A}{g}\cosh(k_1 h) \tag{4.60}$$

after substituting Eq. (4.28) into (4.60) for the selected wavemaker type and the necessary algebraic manipulations, the first-order solution is achieved. For convenience, the first-order solution for the piston-type wavemaker is provided in Hughes (1993):

$$m_1 = \frac{H}{S_0} = \frac{4\sinh^2 kh}{\sinh 2kh + 2kh} \tag{4.61}$$

Substituting Eq. (4.61) into the regular wave expression given in Eq. (4.1) will yield the solution to the first-order piston displacement:

$$X_0^{(1)}(t) = \frac{H}{2m_1}\sin\omega t \tag{4.62}$$

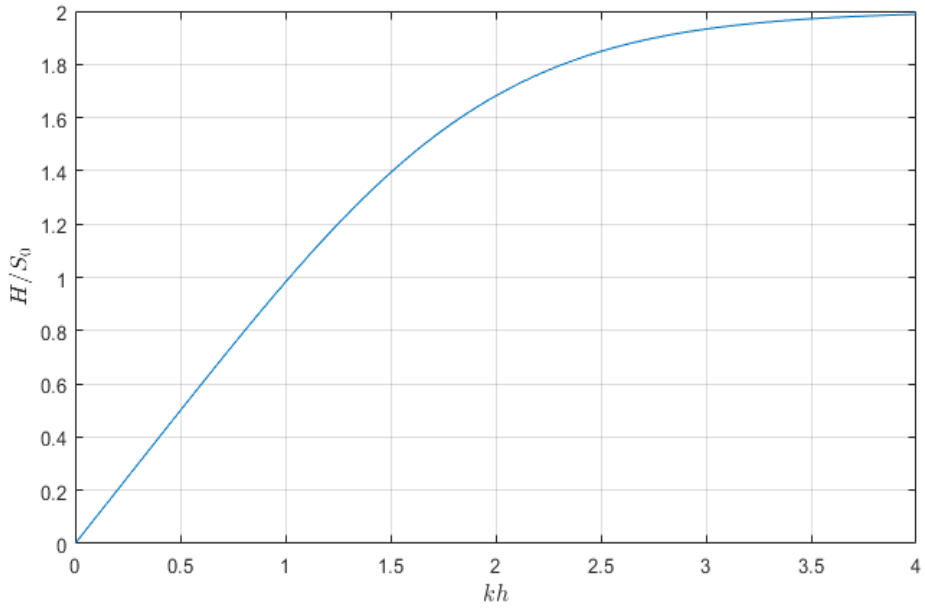

Figure 4.8: Wave height to stroke ratio for the piston-type wavemaker

The phase terms from Eq. (4.1) are not shown for the sake of simplicity. Figure 4.8 shows the wave height to stroke ratio with relative depth for the piston-type wavemaker. It can be seen that the piston-type wave generator's efficiency reaches its maximum at deepwater conditions.

Second-order derivations to the wavemaker problem suggest that the attempts to generate waves in laboratory conditions using the first-order solution will produce unwanted harmonics in the wave flume. It can be seen by observations from Goda (1967) that those spurious-free waves distort the wave record and this effect becomes more dominant as the steepness of the waves H/L increases or the relative depth h/L decreases (Hughes 1993). An approximate second-order wavemaker theory for regular waves developed by Madsen (1970) and Madsen (1971) requiring:

$$\phi^{(2)} = \phi^{(21)} + \phi^{(22)} \tag{4.63}$$

It is worth to reaccent that in this notation $\phi^{(21)}$ describes the second-order bound waves naturally occurring with the wave groups, traveling with the group velocity and $\phi^{(22)}$ describes the spurious effects. The objective of the solution to the velocity potential, $\phi^{(2)}$ is to obtain $\phi^{(23)}$ which gives the relationship in Eq.(4.43). Solving $\phi^{(23)}$ for X_0 will give the wave generator signal required to compensate for the spurious harmonic waves in the generated wave series. Substituting $\phi^{(21)}$ in Eq. (4.63) into the second-order boundary value problems in Eq.(4.45) - (4.47) and substituting $\phi^{(22)}$ in Eq. (4.63) into the second-order boundary value problems in Eq.(4.48) - (4.50) yields two important terms:

$$\phi^{(21)}(x,z,t) = \frac{3\omega H^2}{32}\frac{\cosh 2k(h+z)}{\sin^4 kh}\sin 2(kx-\omega t) \tag{4.64}$$

and,

$$\phi_x^{(22)} = \left(1-\frac{h}{2(h+l)}\right)X_{0_t}^{(2)} + \frac{\omega H^2}{16h}\left(\frac{2}{m_1}-\frac{3\cosh kh}{\sinh^3 kh}\right)\cos 2\omega t \tag{4.65}$$

After solving the boundary value problems for $\phi^{(21)}$ and $\phi^{(22)}$ Madsen (1971) described the second-order wave in terms of the first-order wave, second-order bound wave, and the second-order spurious-free wave. Thus the combined wave board solution becomes:

$$X_0(t) = X_0^{(1)} + X_0^{(2)} \tag{4.66}$$

where $X_0^{(1)}$ is the first-order wavemaker solution given in Eq. (4.62), $X_0^{(2)}$ is the second-order wavemaker solution to compensate for the spurious-free wave, and $X_0(t)$ is the combined second-order wavemaker solution for regular waves. Solution to $X_0^{(2)}$and $X_0(t)$ are given as:

$$X_0^{(2)}(t) = \frac{H^2}{32h\left(1 - \frac{h}{2(h+l)}\right)}\left(\frac{3\cosh kh}{\sinh^3 kh} - \frac{2}{m_1}\right) sin2\omega t \tag{4.67}$$

$$X_0(t) = \frac{H}{2m_1}\sin\omega t + \frac{H^2}{32h\left(1 - \frac{h}{2(h+l)}\right)}\left(\frac{3\cosh kh}{\sinh^3 kh} - \frac{2}{m_1}\right) sin2\omega t \tag{4.68}$$

As an example, a piston displacement solution is provided for the second-order regular wave. Parameters are set as; wave height, $H = 0.2m$, wave period, $T = 5s$, depth, $h = 1m$, solving Eq. (4.3) for the wavenumber, and yields $k = 0.412$. using Eq. (4.2), remaining parameters, angular frequency, and wavelength are obtained as, $\omega = 1.26$, and $L = 15.24m$. Using Eq. (4.52) $m_1 = 0.412$. This is consistent with Figure 4.8, as for very shallow water conditions the relationship is similar to $m_1 \approx kh$. After that, Eq. (4.68) is applied to obtain the necessary wave board motion required to generate the targeted regular wave. The first-order and second-order contributions to the combined wave board motion are also obtained from Eq. (4.62) and (4.67) for demonstration purposes, and they are shown in Figure 4.9.

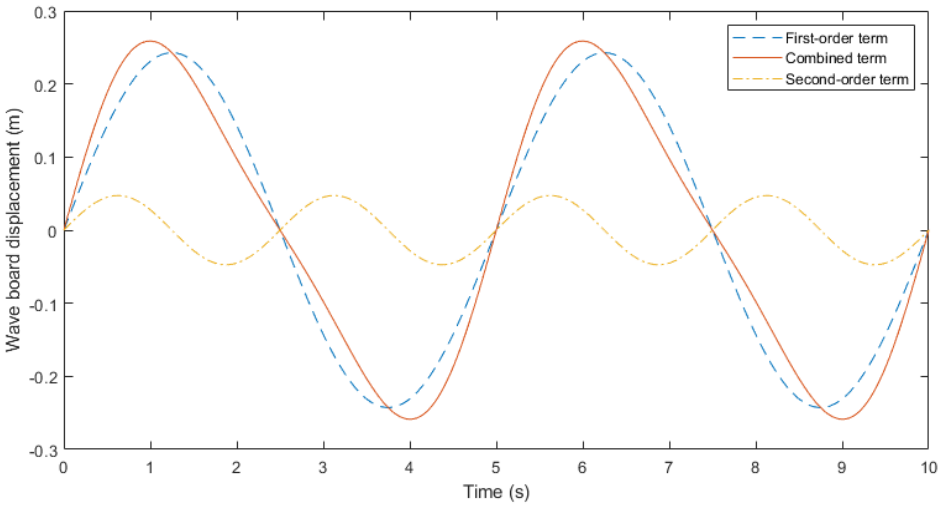

Figure 4.9: Second-order wave board displacement for a regular wave

4.3.2.3. Generation of Irregular Waves

It has been apparent since the earlier attempts to generate first-order irregular waves, second-order harmonic waves also appear in the wave series (Flick and Guza 1980; Ottesen-Hansen 1978; Ottesen-Hansen et al. 1980). Those are both naturally occurring long waves that travel with group velocity as well as unwanted free waves that distort the series. Attempts are made to solve the wavemaker theory boundary value problems to the second-order to acquire necessary transfer functions that compensate those waves to achieve the wave trains that exhibit the targeted properties.

The most widely used approach was to think of the frequencies in the spectral range as the sum (or difference) of two individual monochromatic waves and to solve the equations for every possible frequency combinations for each discrete frequency in the frequency domain. Sand (1982b), Sand and Donslund (1985), and Sand and Mansard (1986) provided solutions for the difference and sum frequencies approach. While the solutions were straightforward, the transfer functions were long and numerous, which makes the user more prone to mistakes and the computational requirements increase exponentially as larger wave series are aimed to be produced. Schäffer (1996) unified the second-order wavemaker theory for both subharmonics (difference frequencies) and superharmonics (sum frequencies) while using a more compact notation and also providing an asymptotic solution method which made his theory both computationally efficient and practical to apply.

The first-order solution Schäffer (1996) provides the transfer function for monochromatic waves which can then be superposed and applied to inverse FFT techniques such as the one given in Section 4.3.1:

$$X_0^{(1)} = \frac{1}{2}\{-iX_a e^{i\omega t} + c.c\} \tag{4.69}$$

where X_a is the constant complex first-order wave board amplitude at still water level and whenever $c.c$ used in the theory, it denotes the complex conjugate of the preceding term. The first-order solution to the boundary value problems Eq. (4.32)-(4.35) is expressed as:

$$\phi^{(1)} = \frac{1}{2}\left\{\frac{igX_a}{\omega}\sum_{j=0}^{\infty} c_j \frac{\cosh k_j(z+h)}{\cosh k_j h} e^{i(\omega t - k_j x)} + c.c\right\} \tag{4.70}$$

$$\eta^{(1)} = \frac{1}{2}\{X_a \sum_{j=0}^{\infty} c_j e^{i(\omega t - k_j x)} + c.c\} \tag{4.71}$$

In the compact notation adopted by Schäffer (1996) the linear dispersion relation for complex numbers are assumed to hold:

$$\omega^2 = g k_j tanh(k_j h) \tag{4.72}$$

Applying eigenfunction expansion to the dispersion equation in Eq. (4.72) yields one real root and an infinity of imaginary roots. Those are denoted as $k_{j=0}$ for the real root and $k_{j>0}$ for the imaginary roots. The real root of the dispersion equation defines the wavenumber for the progressive waves and is denoted as $k_{j=0}$. The imaginary roots are the evanescent modes of the eigenfunction expansion denoted as $k_{j>0}$ which can be obtained by solving (Newman 1990):

$$\omega^2 = -g k_j \tan(k_j h) \tag{4.73}$$

The evanescent modes are the decaying terms that must be obtained from the summation of Eq.(4.73) between $\left[\frac{j\pi}{2}; \frac{j\pi}{2} + \pi\right]$ $for\ j = 1,2,\ldots$ until the solutions converge to zero. Physically, the evanescent modes describe the exponentially decaying local disturbances at the boundary of the wavemaker origin, yet, if ignored, they produce non-decaying free waves (Sand and Mansard 1986). The condition $ik_j > 0$, $j = 1,2,\ldots$ is given for the solution of the dispersion relationship, for the purposes of computational efficiency, and sub-index j is dropped whenever $j = 0$ appears to avoid it to be mistaken as the deep water wave number. Then the first-order transfer function is given:

$$c_j = \left(\frac{\omega^2 h}{g} - \frac{h}{h+l}\right)\frac{1}{D_j(k_j)} + \frac{h}{h+l}\frac{\cosh k_j d}{D_j(k_j)\cosh k_j h} \tag{4.74}$$

where

$$D_j(k_j) \equiv \frac{k_j h}{2}\left(\frac{k_j h}{\sinh k_j h \cosh k_j h} + 1\right) \tag{4.75}$$

then the relationship between the complex amplitude of the first-order wave board, X_a and the complex amplitude of the progressive first-order waves, A is given:

$$A = c_o X_a \tag{4.76}$$

water surface elevation for the progressive first-order waves are described as:

$$\eta_0^{(1)} = \frac{1}{2}\{Ae^{i(\omega t - kx)} + c.c.\} \tag{4.77}$$

and if $A = a - ib$ notation is used, Eq.(4.69) can be described as:

$$X_0^{(1)} = c_0^{-1}(\mathrm{a}\sin\omega t - b\cos\omega t) \tag{4.78}$$

To obtain the wave board motion using the first-order theory, Eq. (4.76) can be interpreted as the relationship between the energy spectrum of the irregular wave to be generated and the wave board motion required to generate it. Since the complex wave amplitude squared will correspond to the magnitudes in spectral density functions, the linear relationship between the irregular wave and the wave board can be defined as (Hughes 1993):

$$S_\eta = c_0^2 S_{wb} \tag{4.79}$$

where S_η denotes the magnitudes in the discrete energy spectrum for the irregular wave series and S_{wb} denotes the magnitudes in the discrete energy spectrum for the wave board motion. This linear interpretation results in a wave board spectrum that have a steep low-frequency tail and a flatter high-frequency tail (Goda 2000) and a comparison of the energy spectra of an irregular wave and the corresponding first-order wave board motion is given in Figure 4.10 that is obtained from this relationship.

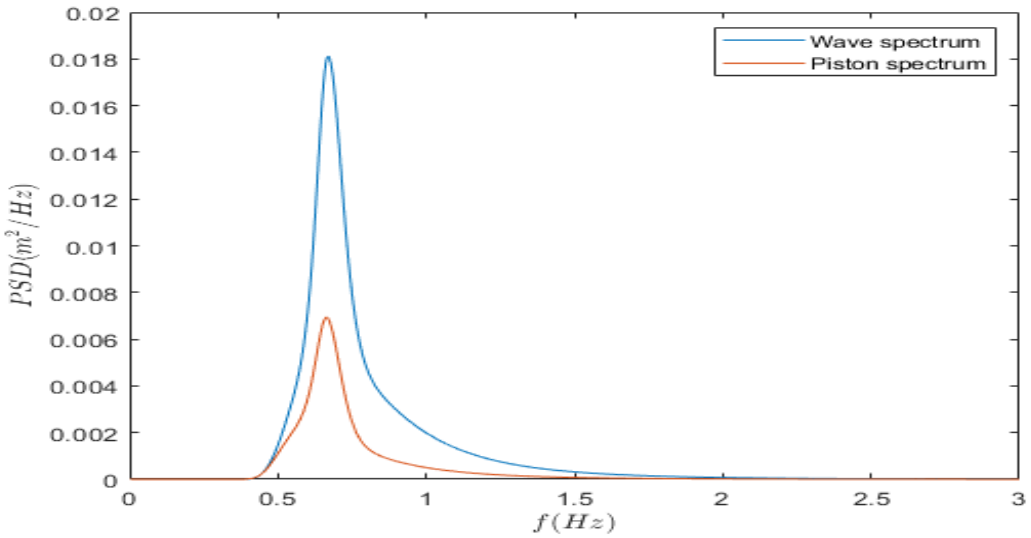

Figure 4.10: Spectra of the targeted irregular wave and the necessary wave board motion to generate it

After that, the wave board motion is obtained using the same synthesis technique that is explained in Section 4.3.1, but using the same randomly generated phases for the irregular waves. An irregular wave and the corresponding first-order wave board displacement example is given in Figure 4.11.

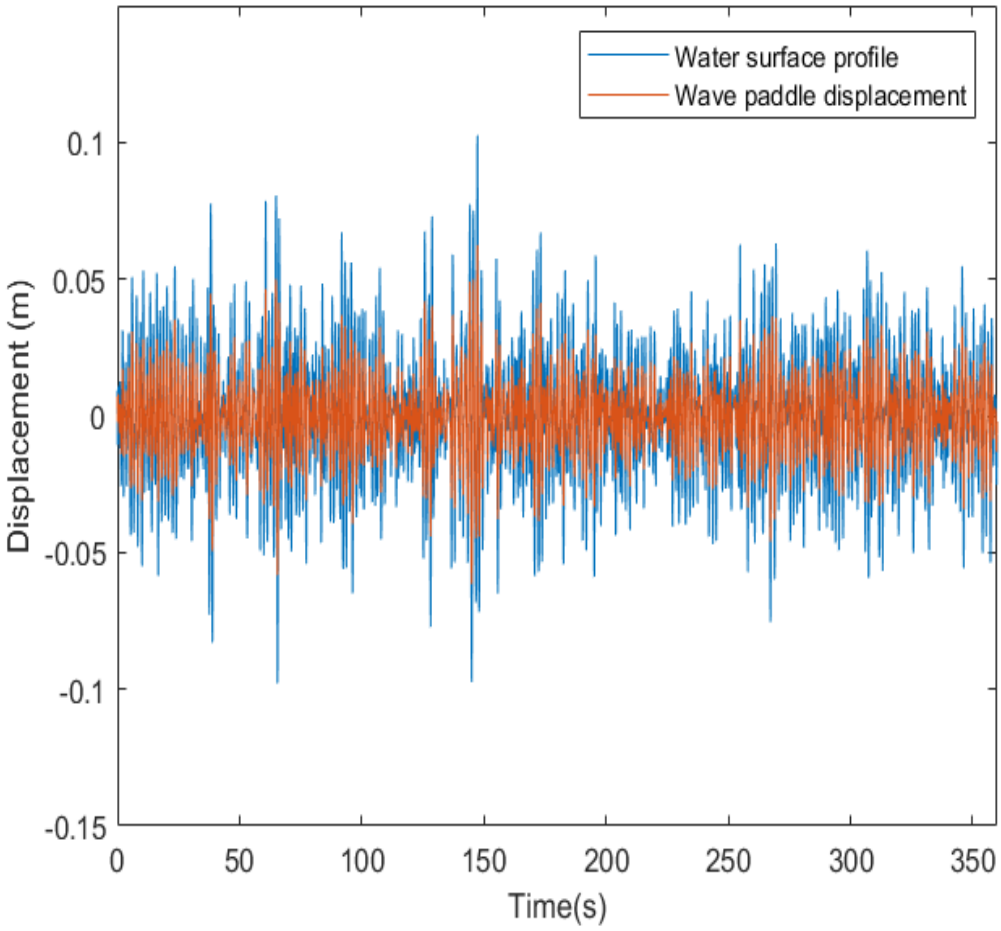

Figure 4.11: An irregular wave series and the corresponding first-order wave board displacement time series

A comparison of the unitless transfer functions for progressive waves and evanescent modes is given in Figure 4.12. It is apparent that the contribution of evanescent modes increase with relative depth and becomes more dominant around $2\pi f\sqrt{h/g} > 3.35$. This underlines the importance of evanescent mode transfer functions when generating waves with a piston-type wavemaker in deep water conditions.

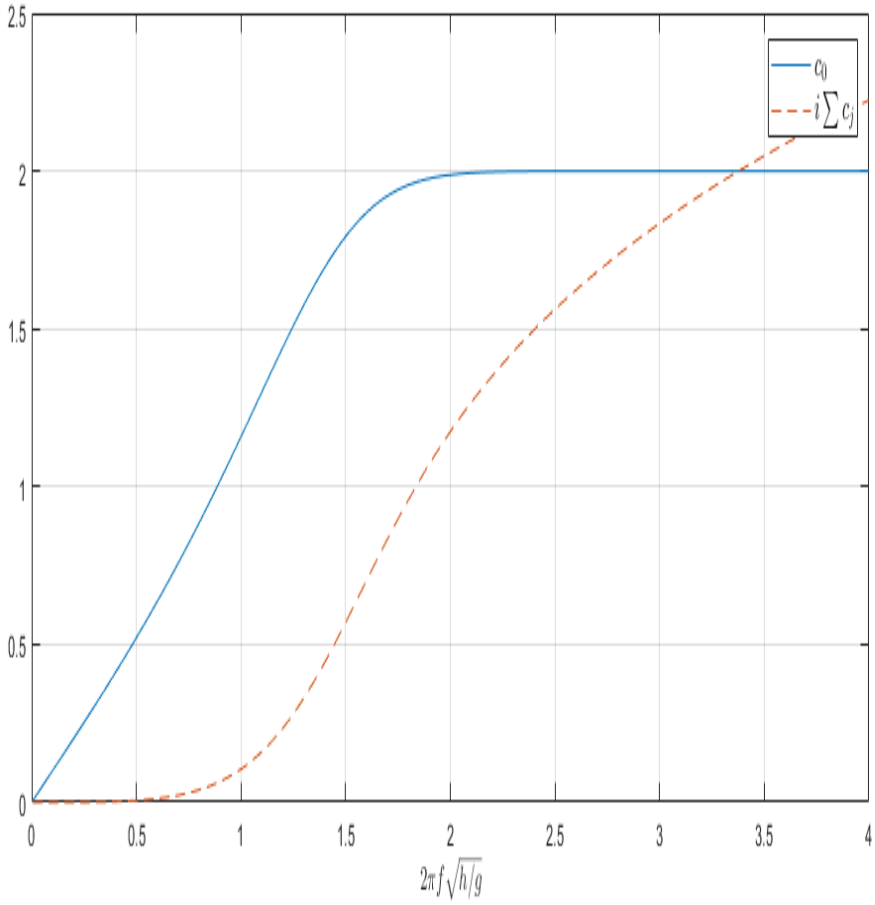

Figure 4.12: Comparison of transfer functions for progressive wave and evanescent modes

In the second-order solution, bichromatic waves are investigated by Schäffer (1996), adopting the notation used in the previous works i.e. (Sand and Mansard 1986). Subscripts m and n are used for properties in respect to the two frequencies that constitute a bichromatic wave. Subscripts l and j are used whenever there is an infinite summation needed such as the calculation of wavenumbers and transfer functions for evanescent modes. Solution to the boundary value problems to the second order is given as:

$$\phi_{jnlm}^{(21)\pm} = \frac{R_{jnlm}^{(21)\pm}}{D_{jnlm}^{\pm}} \frac{\cosh(k_{jn} \pm k_{lm}^{-:*})(z+h)}{\cosh(k_{jn} \pm k_{lm}^{-:*})h} \tag{4.80}$$

$$\eta^{(21)} = G_{jnlm}^{+} X_n X_m^{-:*} c_{jn} c_{lm}^{-:*} e^{i(\theta_{jn} \pm \theta_{lm}^{-:*})} \tag{4.81}$$

$$\phi^{(22)\pm} = \frac{1}{2}\left\{\frac{igA_nA_m^{-:*}}{h(\omega_n \pm \omega_n)}\sum_{p=0}^{\infty} c_p^{(22)\pm}\frac{\cosh K_p^{\pm}(z+h)}{\cosh K_p^{\pm}h}e^{i[(\omega_n\pm\omega_m)t-K_p^{\pm}x]} + c.c\right\} \tag{4.82}$$

$$\eta^{(22)} = \frac{1}{2}\left\{\frac{A_nA_m^{-:*}}{h}\sum_{p=0}^{\infty} c_p^{(22)\pm}e^{i[(\omega_n\pm\omega_m)t-K_p^{\pm}x]} + c.c\right\} \tag{4.83}$$

$$\phi^{(23)\pm} = \frac{1}{2}\left\{\frac{igF^{\pm}A_nA_m^{-:*}}{h(\omega_n \pm \omega_n)}\sum_{p=0}^{\infty} c_p^{(23)\pm}\frac{\cosh K_p^{\pm}(z+h)}{\cosh K_p^{\pm}h}e^{i[(\omega_n\pm\omega_m)t-K_p^{\pm}x]} + c.c\right\} \tag{4.84}$$

$$\eta^{(23)} = \frac{1}{2}\left\{F^{\pm}\frac{A_nA_m^{-:*}}{h}\sum_{p=0}^{\infty} c_p^{(23)\pm}e^{i[(\omega_n\pm\omega_m)t-K_p^{\pm}x]} + c.c\right\} \tag{4.85}$$

where the $+$ and $-$ signs refer to the superharmonic and subharmonic contributions, respectively. The second-order transfer function $F^{\pm}$ and dispersion equation in the form of $K_p^{\pm}$ is given as:

$$(\omega_n \pm \omega_m)^2 = gK_p^{\pm}\tanh K_p^{\pm}h \tag{4.86}$$

$$F^{\pm} = E^{\pm}\left\{\mp\frac{g}{2\omega_n}\sum_{j=0}^{\infty}\frac{c_{jn}k_{jn}^2}{k_{jn}^2-\left(K_0^{\pm}\right)^2}[\omega_n^2-(\omega_n\pm\omega_m)^2] + \widehat{lmjn}^{-:*} + \sum_{j=0}^{\infty}\sum_{l=0}^{\infty} c_{jn}c_{lm}^{-:*}\frac{k_{jn}\pm k_{lm}^{-:*}}{(k_{jn}\pm k_{lm}^{-:*})^2-\left(K_0^{\pm}\right)^2}H_{jnlm}^{\pm}\right\} \tag{4.87}$$

The symbol $-:*$ is used as:

$$Z^{-:*} = \begin{cases} Z\ ;\ for\ superharmonics \\ Z^*;\quad for\ subharmonics \end{cases} \tag{4.88}$$

where $*$ is the complex conjugation of the term. $\widehat{lmjn}$ denotes that the preceding term with jl and mn terms permuted. The solution given for the second-order wave board motion is:

$$X_0^{(2)\pm} = \frac{1}{2}\left[-iF^{\pm}\frac{A_nA_m^{-:*}}{h}e^{i[(\omega_n\pm\omega_m)t]} + c.c\right] \tag{4.89}$$

To validate the code is written, subharmonic and superharmonic contributions of $F^{\pm}$ the transfer function is plotted in Figure 4.13 and compared with the same plots provided in Schäffer (1996), given in Figure 4.14. For more detailed derivations Schäffer (1996) can be referred to.

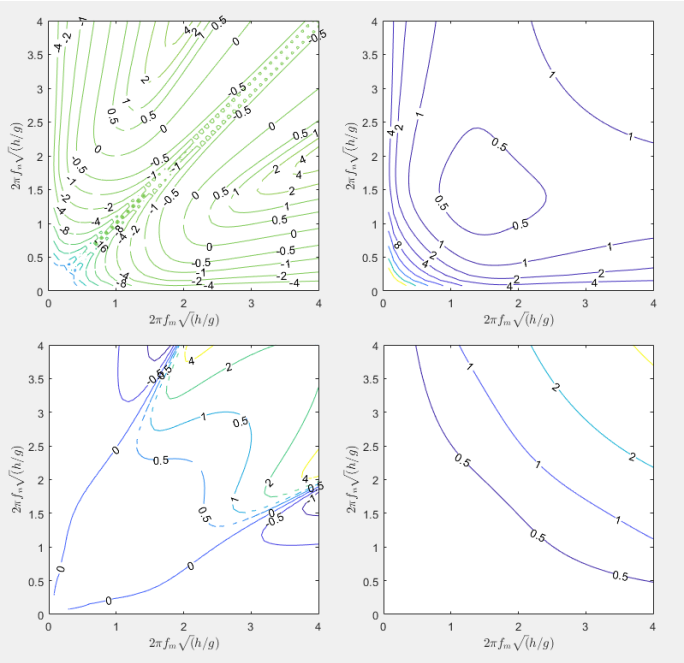

Figure 4.13: Real (upper) and imaginary (lower) components of $F^{\pm}$ transfer function for subharmonic (left) and superharmonic (right) corrections

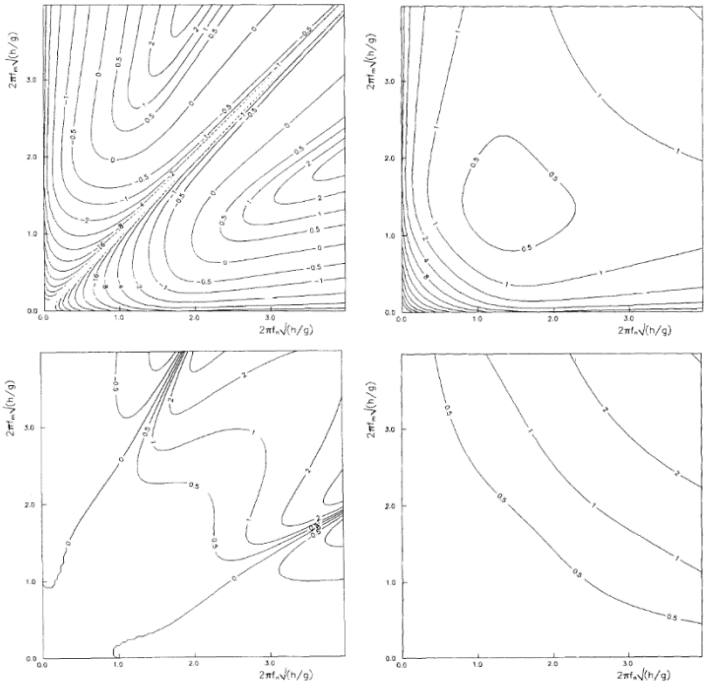

Figure 4.14: Real (upper) and imaginary (lower) components of $F^{\pm}$ transfer function for subharmonic (left) and superharmonic (right) corrections
(source: Schäffer 1996)

4.4. Reflection Analysis

The waves generated by the wavemaker propagate through the wave flume then are reflected by the wall at the end of the flume. Incident and reflected waves are superposed and the time series measured in the flume contain the superposition of the incident and reflected waves. However, there is not such a wall in nature, thus the reflection in the wave channel should be minimized. Moreover, it is necessary to separate the incident waves from the reflected waves in the laboratory measurements because the reflected waves can encounter the waves propagating from the wavemaker and can either enhance or diminish the probe reading.

To separate the incoming waves from the reflected waves, a method developed by Goda and Suzuki (1976) is used. In this analysis method, wave time series measured by two probes that are placed with a specific distance is used. Due to the calculated spectra using the functions derived in the study leads to divergence in an upper and lower boundary of frequencies, wave readings from at least three probes are recommended using this technique.

The premise of this analysis method is the assumption of a wave system that reflects in the wave flume multiple times. The wave generated by the wave board will reflect off the end of the wave flume, then return to hit the wave board and reflect off there. The process continues until the wave energy is absorbed completely. So, the whole system can be described as the superposition of a finite number of waves that propagate along the positive and negative x-axis in the wave flume. Waves propagating along the positive and negative x-direction are termed “incident waves” and “reflected waves”, respectively. The general form of these waves are described as:

$$\begin{aligned} \eta_I &= a_I \cdot \cos(kx - \omega t + \epsilon_I) \\ \eta_R &= a_R \cdot \cos(kx + \omega t + \epsilon_R) \end{aligned} \tag{4.90}$$

where η is the surface profile of the waves, a is the amplitude, k is the wavenumber, ω is the angular wave frequency, and ϵ is the phases. Subindices I and R describe the incident and reflected waves, respectively.

A simple sketch of the wave measurement setup for the reflection analysis is given in Figure 4.15.

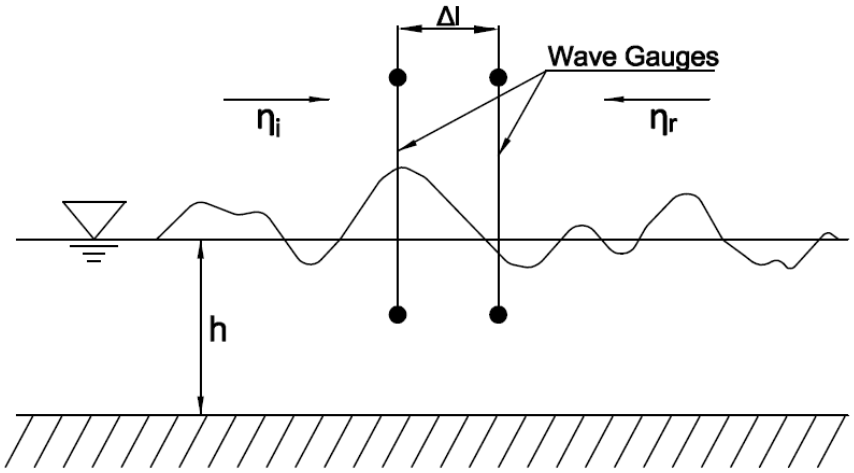

Figure 4.15: System definition for reflection analysis

Surface profile data η_1 and η_2 measured at two consecutive wave gauge probes positioned as x_1 and $x_2 = x_1 + \Delta l$ in the wave flume contain the superposed waves and described as:

$$\begin{aligned} \eta_1 &= (\eta_I + \eta_R)_{x=x_1} = A_1 cos\omega t + B_1 sin\omega t \\ \eta_2 &= (\eta_I + \eta_R)_{x=x_2} = A_2 cos\omega t + B_2 sin\omega t \end{aligned} \tag{4.91}$$

where;

$$\begin{aligned} A_1 &= a_I cos\phi_I + a_R cos\phi_R \\ B_1 &= a_I sin\phi_I - a_R sin\phi_R \\ A_2 &= a_I \cos(k\Delta l + \phi_I) + a_R \cos(k\Delta l + \phi_R) \\ B_2 &= a_I \sin(k\Delta l + \phi_I) - + a_R \sin(k\Delta l + \phi_R) \end{aligned} \tag{4.92}$$

and,

$$\begin{aligned} \phi_I &= kx_1 + \epsilon_I \\ \phi_R &= kx_1 + \epsilon_R \end{aligned} \tag{4.93}$$

Solving Eq. (4.92) yields;

$$\begin{aligned} a_I &= \frac{1}{2\left|\frac{sin2\pi\Delta l}{L}\right|}\sqrt{(A_2 - A_1 cosk\Delta l - B_1 sink\Delta l)^2 + (B_2 + A_1 sink\Delta l - B1 cosk\Delta l)^2} \\ a_R &= \frac{1}{2\left|\frac{sin2\pi\Delta l}{L}\right|}\sqrt{(A_2 - A_1 cosk\Delta l + B_1 sink\Delta l)^2 + (B_2 - A_1 sink\Delta l - B1 cosk\Delta l)^2} \end{aligned} \tag{4.94}$$

The dispersion relationship in Eq. (4.3) is used in the calculations. In the analysis of regular waves A_1, A_2, B_1, B_2 coefficients are calculated with Fourier analysis. Then, the amplitudes of the incident and reflected waves can be found with Eq. (4.94).

It is possible to analyze irregular waves with the assumption that the irregular waves can be described as the superposition of an infinite number of regular waves. A_1, A_2, B_1, B_2 coefficients can be calculated with fast Fourier transform, then applying Eq. (4.94) gives the discrete a_I and a_R amplitudes. A closer look at Eq. (4.94) will reveal that when $\frac{\Delta l}{L} = 0.5 \cdot n,\ \ n = 0,1,2,\ldots$ Eq. (4.94) has no real solution. Calculation of incident and reflected waves are impossible at the points. Therefore the distance between the two wave gauges should be determined accordingly For example, in a laboratory setup where gauge 1 and gauge 2 are 0.2m apart from each other and the wave has deep water characteristics, a test wave with 2Hz frequency will have a wavelength of $L \cong 0.4m$ and between gauges 1-2: $\frac{\Delta l}{L} \cong 0.5$, so the reflection analysis is impossible to perform.

For the irregular waves the criterion for the positioning of the wave gauges is given as:

$$f_{min}: \frac{\Delta l}{L_{\max}} = 0.05$$
$$f_{max}: \frac{\Delta l}{L_{\min}} = 0.45 \qquad (4.95)$$

where $L_{\max}$ and $L_{\min}$ are the maximum and minimum wavelengths and are calculated according to f_{min} and f_{max}, respectively. Analysis of the wave measurements is restricted between the minimum and maximum frequencies. However, there is a possibility that the effective range may be taken slightly wider than that given by Eq. (4.95) e.g., f_{min} may be chosen so that $\frac{\Delta l}{L_{\max}} = 0.03$ (Goda and Suzuki, 1976).

Next, wave energies are calculated for the incident and reflected waves in the range of f_{min} to f_{max}:

$$E_I = \int_{fmin}^{fmax} S_I(f)df$$
$$E_R = \int_{fmin}^{fmax} S_R(f)df \tag{4.96}$$

The reflection coefficient can be calculated with the ratio between the incident and reflected waves:

$$K_R = \sqrt{\frac{E_R}{E_I}} \tag{4.97}$$

Wave heights of the incident and reflected waves are derived from spectral moments:

$$H_I = \frac{1}{\sqrt{1+K_R^2}} H_S$$
$$H_R = \frac{K_R}{\sqrt{1+K_R^2}} H_S \tag{4.98}$$

For instance, an irregular wave set is measured at a water depth of $0.885m$. and the peak wave frequency is found to be 0.75Hz. The energy spectrum is plotted and it is seen that the wave energy lies between the upper and lower boundaries of $0.5 * f_p$ and $2 * f_p$, respectively. The wavelengths for the minimum and maximum frequencies are calculated as $L_{max} = 7.5m$ and $L_{min} = 0.7m$, respectively. By applying the in wavelengths in Eq. (4.95) wave gauge spacing may be chosen between 0.225m and 0.315 and it is set to $\Delta l = 0.3m$. Wave gauges are set apart to the designated distance and wave measurements are taken for reflection analysis. After the application of zero up crossing, superposed significant wave heights are calculated as $0.121m$, and $0.104m$. Then, FFT is applied to calculate the Fourier coefficients of measured waves, and using Eq. (4.94), amplitudes of the incident and reflected waves are calculated. Spectral resolution for the incident, reflected, and composite waves are given in Figure 4.16, and the effective range of resolution is shown. As stated above, the figure shows the divergent frequency limits, f_{min} and f_{max}. So, in order to achieve a wider range of frequencies to analyse, wave measurements from more than two wave probes should be used.

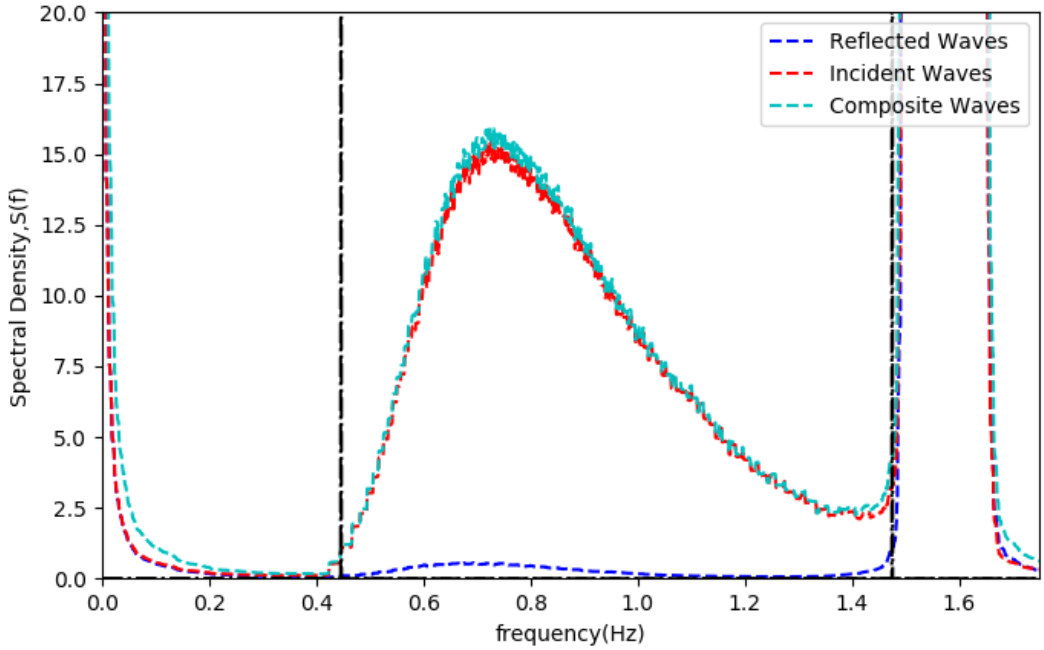

Figure 4.16: Spectral resolution in the effective range of frequencies

In Figure 4.16, the area under each wave type is equal to the wave energy described in Eq. (4.96). Lastly, Eq. (4.97) and (4.98) are applied to calculate the reflection coefficient and found as $K_R = 0.181$, and the incident and reflected wave heights are calculated as $H_I = 0.11m$, and $H_R = 0.02m$, respectively.

CHAPTER 5

LABORATORY SETUP FOR PHYSICAL MODEL EXPERIMENTS OF THE SPAR-TYPE FLOATING OFFSHORE WIND TURBINE

5.1. Wave Flume Setup

The laboratory experiments are being conducted in a wave flume of 40 m length, 1 m width, and 1.40 m depth. The flume was constructed from steel but a part with 8m length was covered by thick glass to make visual observations during the experiment. The general view of the wave flume is shown in Figure 5.1

Figure 5.1: Laboratory wave flume

In the experimental study, the selection of the model scale is very important. Since the small scales cause erroneous results, the purpose is to select the largest scale possible for the experiments. However, there are some constraints. For example, the maximum water depth is 1m in the wave flume. Nevertheless, deeper water is necessary for the experiments since a FOWT will be modeled. Therefore, a trade-off between the water depth and the scale effects brought the result of selecting the scale as 1/40. At the beginning of the wave flume, a piston-type wave generator was built to generate waves. The wave generator runs on a 5-kW, 2000rpm AC servo motor. The servo motor is connected to a ball screw shaft which holds a vertical plane called the wave board. The revolutions of the servo motor are converted to the linear motion that drives the wave board back and forth in the wave flume. The motion of the wave board forces oscillations on the water surface that imitates natural waves. During the experiments, the piston-type wave generator uses the wave board displacement time series,(see Chapter 4), which are then converted to the driving signal for the servo motor of the wave generator. The design, construction, and generation of the servo motor driving signal are not in the scope of this study. A detailed view of the wave generator is given in Figure 5.2 and Figure 5.3

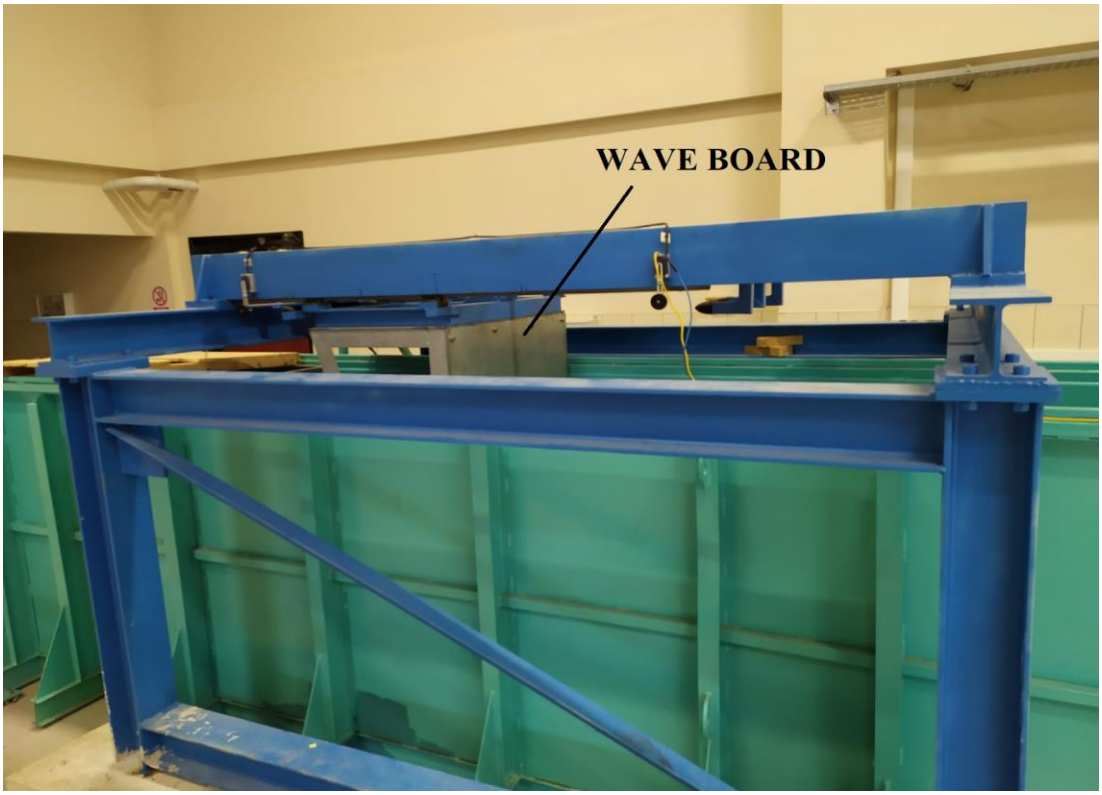

Figure 5.2: Side view of the piston-type wave generator

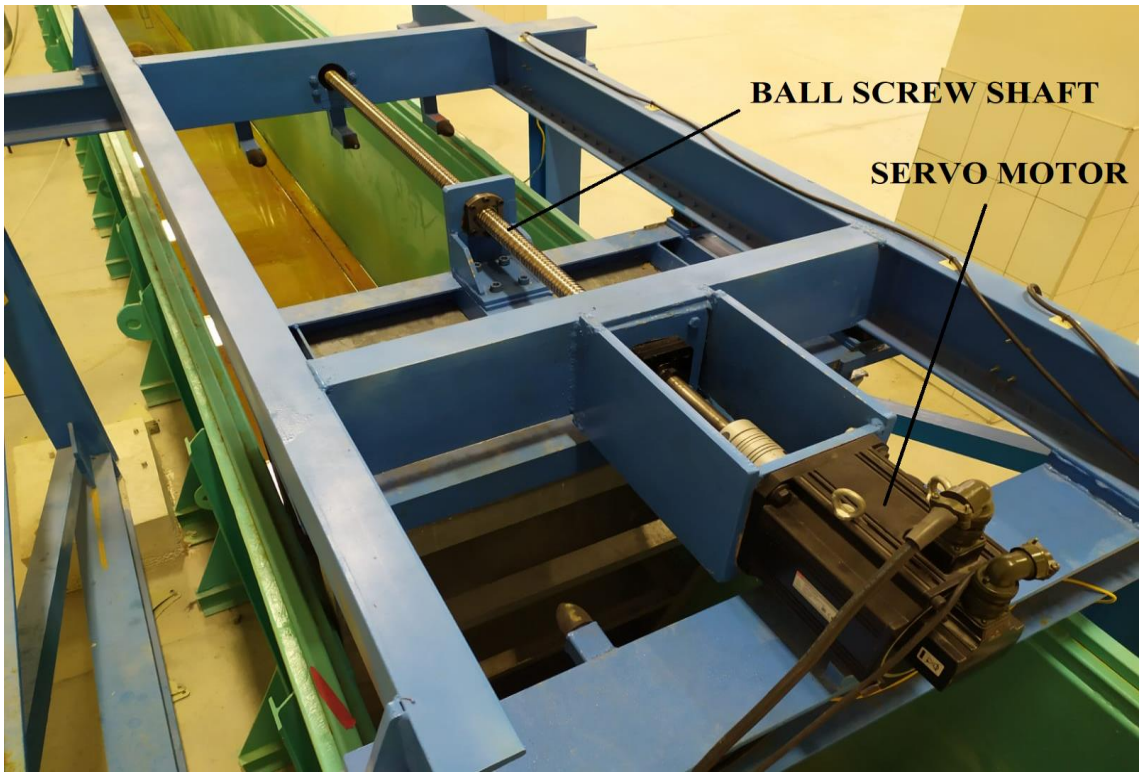

Figure 5.3: Top view of the piston-type wave generator showing the servo motor and ball screw shaft

At the middle of the wave flume, a wind nozzle is mounted on the wave flume to obtain the wind profiles that represent the atmospheric boundary layer. The wind nozzle is shown in Figure 5.4

Figure 5.4: Wind nozzle and connected fans

The wind nozzle has a 4-to-1 contraction ratio, the entrance and outlet dimensions of the wind nozzle are 180x180cm and 90x90cm, respectively, with a length of 360cm. The wider entrance connects to 4 fans with individual speed control to mimic the gradual increase that resembles the logarithmic wind profiles in nature. Additionally, a layer of perforated screen and a layer of honeycomb are placed inside the wind nozzle to minimize the turbulence of the wind flow. For the details in the design and construction of the wind generation system Erol (2020) can be referred to.

5.2. Model set-up

The essence of physical model experiments is creating a model environment that behaves as a scaled-down representation of the prototype. To obtain that model, similarity laws must be obeyed. Similarity laws can be divided into three categories (Goda 2000):

-Geometric Similarity: Geometric similarity is achieved when all the lengths in the model are the same ratio to the respective lengths in the prototype in all three dimensions. In other words, the length-scale ratio is kept constant between the model and the prototype.

-Kinematic Similarity: Kinematic similarity is achieved when length-scale and time-scale ratios between the model and the prototype are kept constant. Consequently, velocity and acceleration terms between the model and prototype will be properly scaled.

-Dynamic Similarity: Dynamic similarity is achieved when all the forces between the model and the prototype have a constant ratio. In other words, length, time, and force scales are kept constant between the model and the prototype.

For the physical modeling of the spar-type floating offshore wind turbine platform, similarity laws are obtained by keeping the Froude number constant between the model and the prototype (i.e. Froude similitude) since it provides proper scaling of the inertial and gravitational forces, which are dominant in the problem (Martin et al. 2014b). A length scale of 1/40 is chosen considering the laboratory conditions.

Froude scale factors are given for relevant parameters for $\lambda = \frac{L_{model}}{L_{prototype}} = 1/40$ in Table 5.1:

Table 5.1: Froude scale factors for the laboratory experiments

Parameter	**Scale factor**
Length	λ
Area	λ^2
Volume	λ^3
Angle	1
Time	$\sqrt{\lambda}$
Frequency	$\sqrt{\lambda}^{-1}$
Density	1
Mass	λ^3
Velocity	$\sqrt{\lambda}$
Acceleration	1
Force	λ^3
Moment	λ^4
Stress	λ
Mass moment of inertia	λ^5
Mass per unit length	λ^2
Modulus of Elasticity	λ

The properties of the floating offshore wind turbine and the mooring system are given for the prototype and the model in Table 5.2 and Table 5.3, respectively.

Table 5.2: Floating offshore wind turbine properties

Property	**Value (Prototype)**	**Value (Model)**
Mass	1.17e+06 kg	18.27 kg
Draft	27.04 m	0.68 m
The volume of displaced water	1177.4 m^3	0.0184 m^3

(cont. on next page)

Table 5.2 (cont.)

Center of mass below SWL	18.63 m	0.466 m
Center of buoyancy below SWL	15.44 m	0.39 m
Roll inertia	2.04e+08 kg·m^2	2.00 kg·m^2
Pitch inertia	2.04e+08 kg·m^2	2.00 kg·m^2
Yaw inertia	6.20e+06 kg·m^2	0.06 kg·m^2
Static buoyancy force	1.16e+07 N	180.48 N
Heave hydrostatic stiffness	4.80e+04 (30.02) N/m	30.02 N/m
Roll hydrostatic stiffness	6.43e+05 N·m/°	0.25 N·m/°
Pitch hydrostatic stiffness	6.43e+05 N·m/°	0.25 N·m/°

Table 5.3: Mooring system properties

Property	**Value (Prototype)**	**Value (Model)**
Type	Catenary studless chain	Catenary studless chain
Mass per unit length in air	121.07 kg/m	0.076 kg/m
Mass per unit length in water	112.01 kg/m	0.070 kg/m
Nominal diameter	0.0779 m	0.002 m
Equivalent diameter	0.1404 m	0.0035 m
Stiffness, EA	5.1989e+08 N	8.1232e+04 N
Angle between lines	120°	120°
Cable pretension	3.1e+05 N	0.48 N
Radius to fairlead from the centerline	4.0 m	0.11 m
Radius to anchor from the centerline	300 m	7.5 m
Cable length	306.5 m	7.66 m
Initial laid cable length	277.67 m	6.94 m

The prototype design of the spar platform is done by Alkarem (2020) using the OC3 Hywind® concept (Jonkman 2010) as a reference. For the model, geometric similitude is achieved and the platform dimensions are obtained using the 1/40 Froude scale. Due to the length scale of the experiments, the floating platform will simulate a water depth of 40 meters. In the prototype design spar platform shell material is

stainless steel and a studless chain is used for mooring lines. Since dynamic similitude is aimed, mooring lines in the model are produced using the same material with mass per unit length scaled with λ^2 scale factor and spar platform shell material are constructed with the same stainless steel material, keeping the density scale factor of "1". In the prototype design concrete ballast is used, but, due to practical issues, ballast type is decided as a mix of sand or water that has the same density as the concrete. The constructed spar-type platform model is shown in Figure 5.5, and its dimensions are given in Figure 5.6.

Figure 5.5: Scaled model of the spar-type floating platform with one mooring chain attached

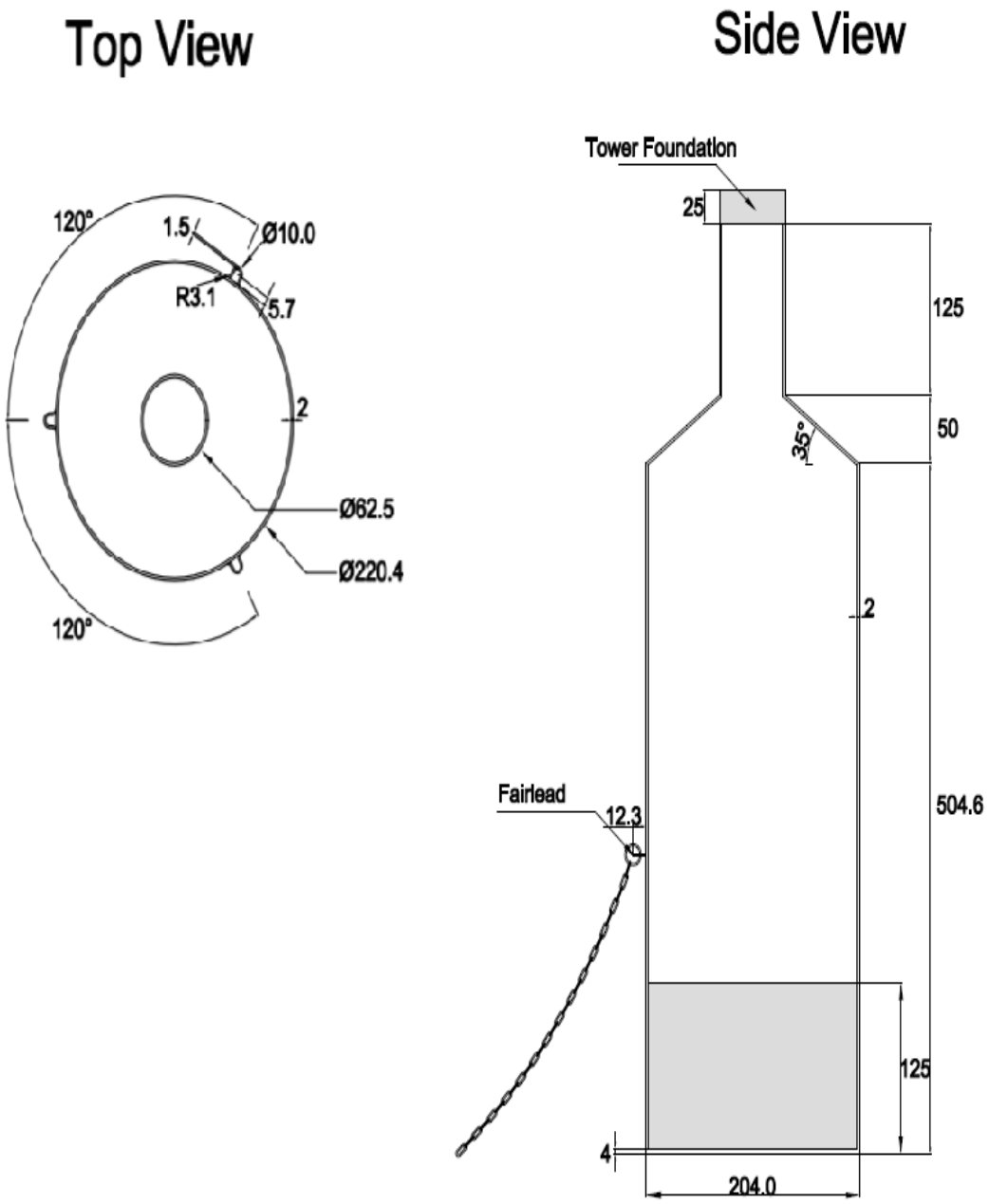

Figure 5.6: Dimensions of the scale model of the spar-type floating platform

The mooring system of the FOWT design has the same symmetry (120°) as the OC3 model. However, due to the limitations in the wave flume dimensions, two mooring cables downwind of the model can't be laid as designed. The lengths of the mooring lines could not be kept short as this would result in extra stiffness. To circumvent this problem, a pulley system is produced and placed on the side walls in the wave flume, allowing the designed symmetry of the cables while keeping design

parameters and the stretching-loosening ability of the mooring lines intact. The pulley system is shown in Figure 5.7.

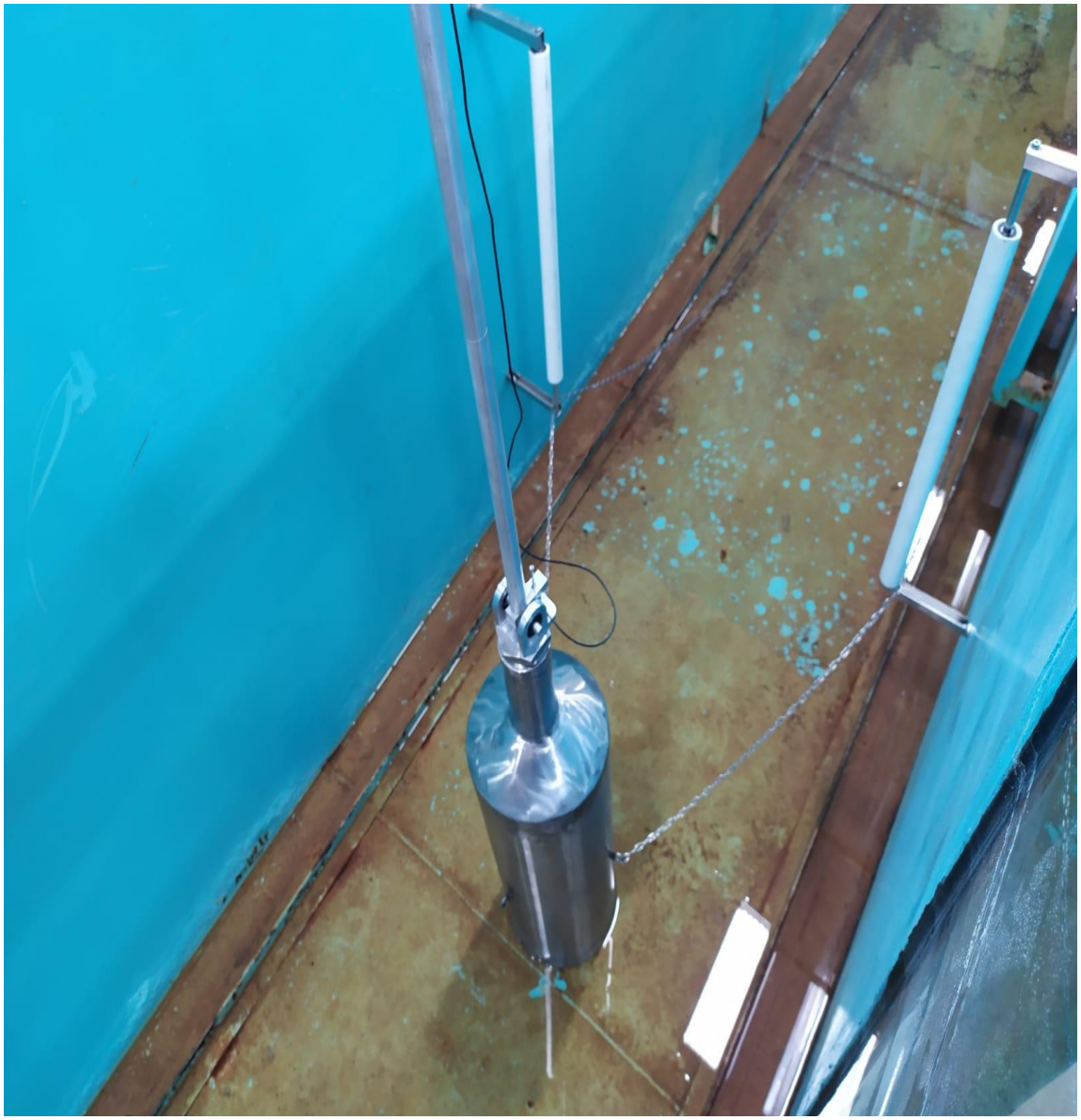

Figure 5.7: Pulley system for the leeward mooring lines

The experimental model setup is an ongoing process. Currently, the wave measurement system is fully implemented and functional (see. Section 5.3), and both regular and irregular waves can be generated and measured in the wave channel. The devices to measure the tension forces on the mooring cable and to capture the motion responses of the spar-type floating offshore wind turbine under regular and irregular waves are not implemented yet and planned for the near future.

A top-down sketch of the wave flume setup is given in Figure 5.8:

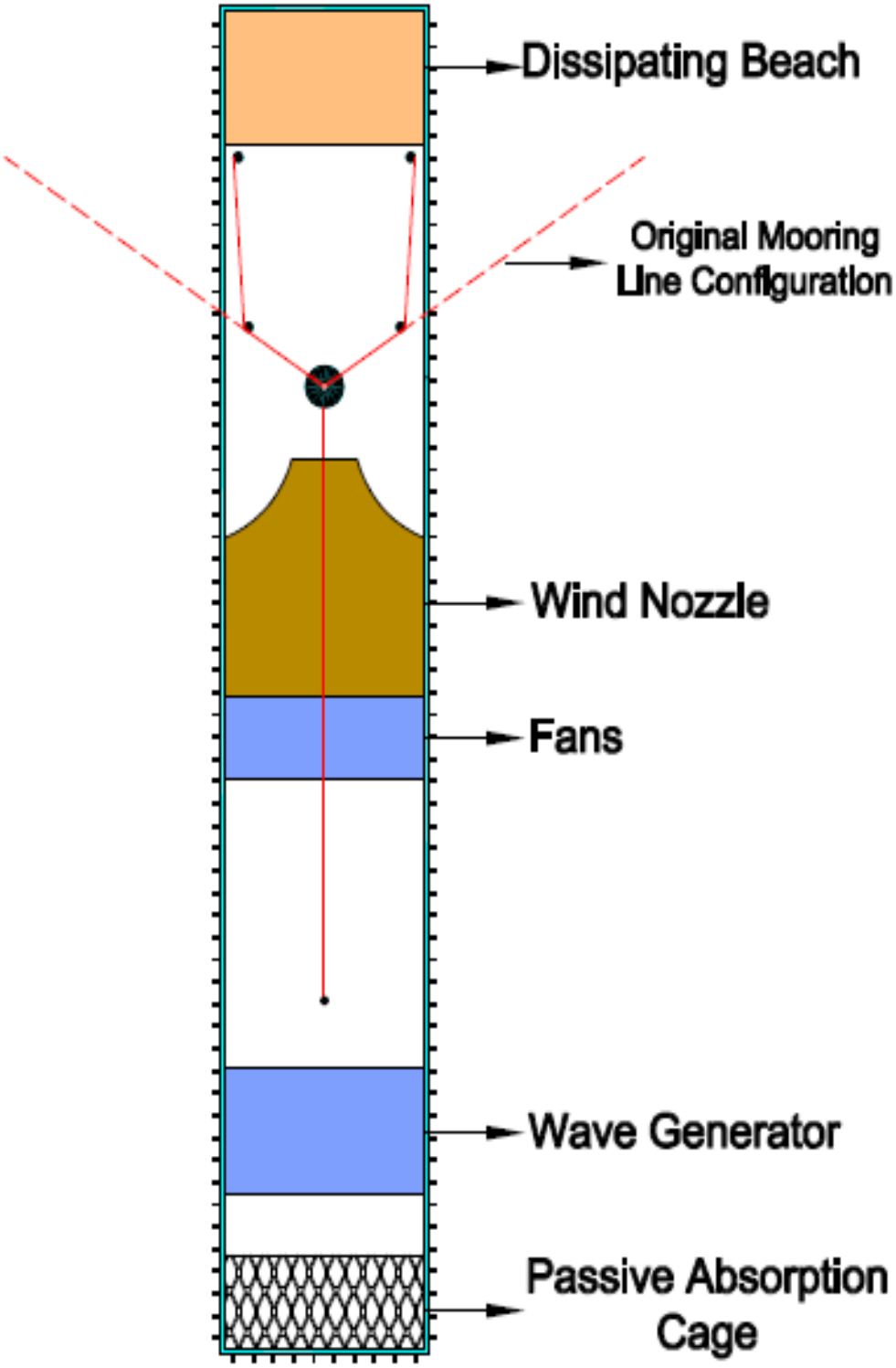

Figure 5.8: Top-view sketch of the wave flume

5.3. Wave Measurement and Analysis

As explained in Chapter 4, Using the wavemaker theory, a code is written to produce the wave signal for the wave generator. Therefore, it is possible to generate regular or irregular random wave series in the laboratory wave flume (see Section 4.3). To use the waves produced by the piston-type wave generator, wave measurements need be to taken and compared with the waves that were generated theoretically.

Waves are measured using the HR Wallingford Wave Measurement System™ which consists of 60 cm twin wire analog wave probes and a wave gauge monitoring device with a built-in 16 bit A/D converter. The wave probes can be described as a steel wire that acts as a resistor when submerged in water. While the wave probes operate, the current that flows between the wires is converted to the output voltage and logged in the wave gauge monitor. If the probes are submerged further, or the probes encounter the wave crest, the resistance will shorten, producing an increase in the output voltage, vice versa.

The data logged in the wave gauge monitor are analyzed in Python using the code that is written in house. Wave probes are mounted on wooden planks to make the re-location practical. Images of the mounted wave probes and the wave gauge monitor are shown in Figure 5.9 and Figure 5.10, respectively.

The analog readings measured by the wave probes are transferred to the wave gauge system in the observation room. The wave gauge measurement system converts the analog reading to digital data using a built-in 16-bit A/D converter. The digital output is then converted to wave heights in cm unit using the transfer functions derived from calibration.

The wave gauge measurement system has an output voltage between -10V and +10V. The voltage data is read on the data acquisition software and can be logged in the computer that is connected to the wave gauge measurement system. The voltage data that is logged is read using a Python code written in-house. The voltage readings can be converted to water surface profile measurements in length units using the conversion equations obtained by the calibration of the wave probes.

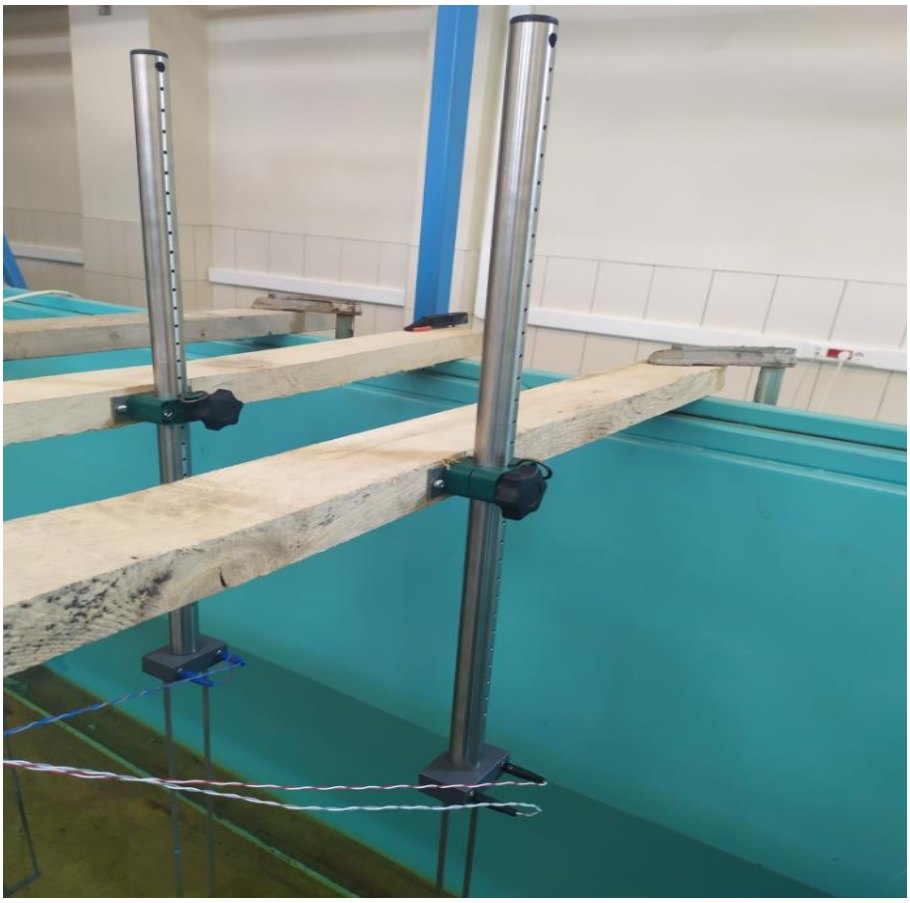

Figure 5.9: Wave probes, mounted on the wave flume

Figure 5.10: Wave gauge monitor

5.3.1. Calibration & Measurement

To convert the voltage differences to the water surface profile, calibration should be done daily before the start of the experiment. The calibration scheme is as follows (HR Wallingford, 2015):

-After the probes are placed at the designated locations, analog gain for every probe is changed so that it shows 0 in still water level.

-The expected maximum wave height is considered and the calibration range is set to higher bounds to catch the trough and crest of the maximum wave

-Voltage data are read for each probe at still water level and recorded

-Measurement range is divided into steps

-Starting from SWL, probes are moved downwards in pre-designated steps, for each step, voltage readings are noted

-When the maximum depth range is reached, probes are moved upwards in pre-designated steps and voltage readings are noted for each step

-At the point of minimum depth for the probes, the same procedure is repeated downwards until the wave probe reached its initial position in SWL

-Recorded voltages are plotted and formulas that convert the probe voltage to wave height for each wave gauge are obtained using linear regression.

An example for the calibration of a wave probe is given in Table 5.4 and Figure 5.11, readings are taken at SWL for -12, -6, 0, 6, 12 cm depths:

Table 5.4: Wave probe calibration example

Wave probe voltage reading (V)	Submerged depth of the probe from the reference point (cm)
0.003	0
2.171	6
4.367	12

(cont. on next page)

Table 5.4 (cont.)

2.164	6
-0.004	0
-2.088	-6
-4.125	-12
-2.095	-6
-0.003	0

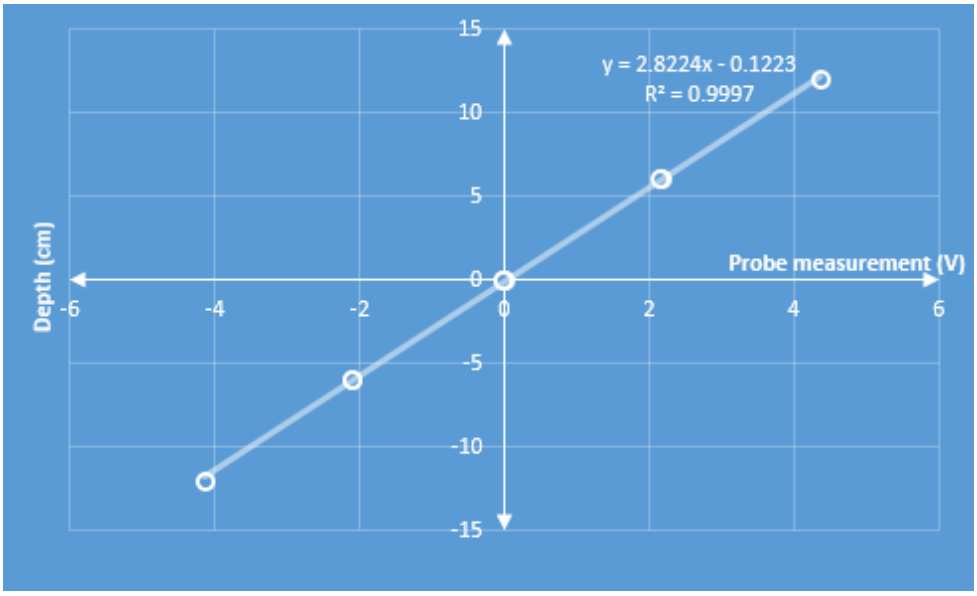

Figure 5.11: Linear regression to obtain the depth-voltage relationship

Conversion formulas are obtained after performing calibration for each probe. In the experiments, the measurements taken are logged into a text file using the built-in software of the wave gauge monitor, which are then analyzed using the code written in Python for this purpose.

An example of an irregular wave measurement taken in the wave flume is given with spectral properties, $H_s = 12.5\,cm$, and $T_p = 1.5\,s$. After obtaining the irregular wave time series and the piston displacement matrix, the data is converted to the driving signal for the wave generator. After waiting a sufficient time for the first re-reflected waves from the wave board to reach the wave probe, measurements are taken for at least a hundred wave periods as described in Goda (2000), the voltage data is logged to a text file and analyzed in the Python code. The first sixty seconds of the irregular wave

measurement is given in Figure 5.12. The zero-up crossing yields $H_s = 12.46\,cm$ and $T_s = 1.60\,s$. The wave parameters are found to be quite close to the targeted characteristics.

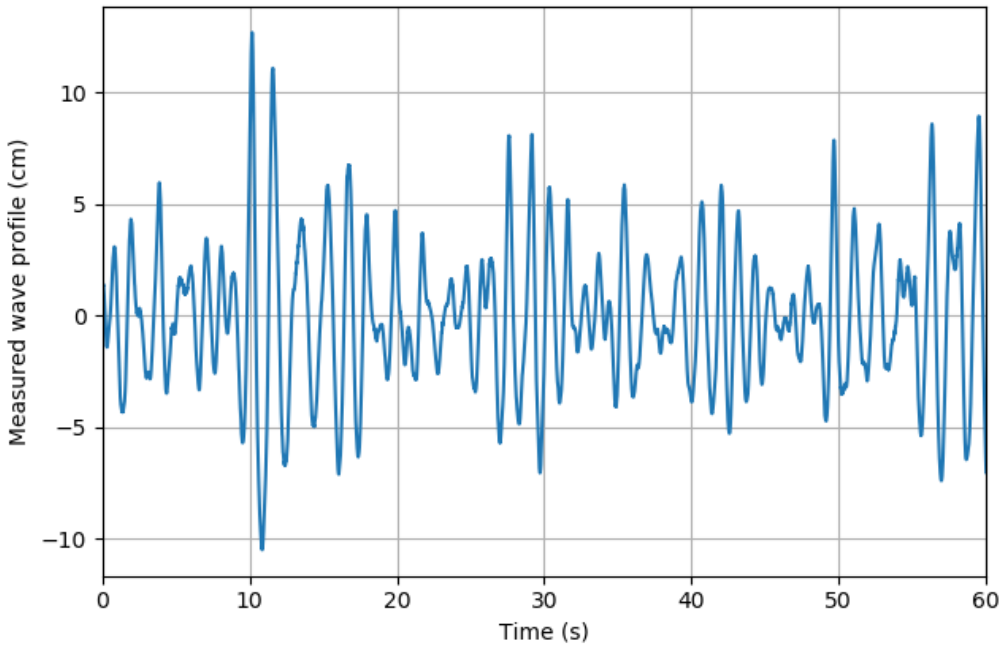

Figure 5.12: Irregular wave measurement taken in the wave flume

5.4. Passive Absorption of the Reflected Waves

A well-known problem in physical experiments in wave flumes is the reflection. The waves propagating forward reflect off the wall at the end of the flume, then return to the wave board and reflect off towards the forward end of the channel again, until the wave energy dissipates completely. The reflections and re-reflections can distort the wave record and result in inconsistencies in the experiments. One way to circumvent this problem is the burst method (Madsen 1970) where a burst of waves is generated and measured until the reflections become effective in the wave record. The first few waves of the burst waves will also be removed from the record due to the wave board starting its motion from rest producing larger waves. In this study, this method is used in the initial tests of the regular wave generating capabilities of the wave generator.

However, the load cases for the FOWT model requires wave trains to be generated on much longer time periods. Therefore, a dissipating beach consisting of rocks of varying sizes is laid at the end of the channel with a 1/5 slope to mitigate the reflections occurring in the wave flume. The dissipating beach is shown in Figure 5.13.

Figure 5.13: Dissipating beach

In addition to the reflection problem at the end of the channel, there is a similar problem at the beginning of the channel at the back of the generator. Since the water is present at both sides of the wave board, waves propagate to the backward of the board and create splashes of water that cause risks of damaging the motor when the generated and reflected waves overlap. Thus, a steel cage filled with an absorbing material (plastic sponges) is placed at the back of the generator to absorb the wave energy there. (see Figure 5.14). It is observed that the plastic sponge material absorbs much of the wave energy and eliminates the risk of damaging the motor.

A much better way to deal with reflection would be achieved by the active absorption of the reflected waves. In active absorption systems, the reflected waves are

absorbed by a device that is similar to the wave board that produces progressive waves in the wave flume. Placed at the reflecting end of the flume, this device should force the incoming waves in a way that absorbs them, instead of reflecting them (Dean and Dalrymple 1984). However, considering the dissipating beach laid at the end of the flume, there is no room for such a system.

Figure 5.14: The wave absorbing steel cage

Another approach to active absorption is “the absorbing wave board” which lets the wave generator perform the absorbing motion whenever the reflected waves arrive. To implement this method, real-time force measurements on the wave board using force transducers (Hughes 1993) or real-time water surface elevation near the board (Schaffer and Jakobsen 2003) is necessary. Either way, to implement such a system, an active feedback control system needs to be established. The implementation of active absorption capabilities is aimed at the piston-type wave generator in the future.

CHAPTER 6

CONCLUSIONS

A numerical model is investigated to gain inference on the dynamic response of a spar-type floating offshore wind turbine under regular and irregular wave loads. Floating spar-type platform supporting a 5-MW baseline wind turbine and the catenary mooring lines that anchor the structure to the seabed is modeled, taking the specifications provided in OC3 Phase IV code collaboration comparison. Wind loads and servo-elastic behavior of the FOWT is kept out of scope. The obtained results show agreement with the other participants' results in OC3. Investigation of the system response under wave loads provided valuable information regarding the stability performance of the spar model. It is inferred from the results that the spar model performs best in heave DOF, staying virtually unaffected from the wind loads. However, surge and pitch responses of the model showed that the model is indeed quite vulnerable to wave loads in these degrees of freedom, so, the natural frequencies in pitch and surge should best be away from the peak frequency of the wave spectrum.

Aiming to prepare the laboratory wave environment necessary to conduct physical model experiments in the wave flume located in the hydraulics laboratory in IZTECH, efforts are made in the production of a wave generator with regular and irregular wave generation capabilities. The investigation of the established wavemaker theory revealed that the correct reproduction of naturally occurring waves is not possible using the first-order solutions of velocity potential in the boundary value problems at the wavemaker. In fact, due to the assumptions at the wave board, first-order wave board motion produces spurious waves at low frequency and high-frequency regions of the spectrum, termed subharmonics and superharmonics, respectively. The second-order corrections for both regular and irregular waves are investigated and transfer functions are provided in this study, with the inclusion of an iFFT method used to apply the corrections to the wavemaker code written for the laboratory wave generator. As of the writing of this thesis, second-order regular wave generation is fully implemented in the piston-type wave generator in the wave flume, and while the second-order irregular wave generator code is completed, it is not encoded in the wave

generator and tested yet. However, by taking into consideration the results obtained in the numerical investigation of the OC3 spar model, which revealed that the natural frequencies of the floating structure lie in the low-frequency region, it is possible to deduce that the second-order effects, especially subharmonic waves will influence the motion response of the floating platforms considerably and the elimination of the spurious harmonic waves is of utmost importance.

The wave flume is prepared for testing the waves generated by the piston-type wave generator located in the flume. The theoretically generated waves are transformed into the wave board position matrix in the time domain that is required to create the targeted wave series. The position matrix is then converted to the driving signal for the AC servo motor which oscillates the wave board. The conversion of the wave board position to the motor signal is out of scope for this thesis. However, an integrated graphical user interface is created and used to run the codes generating the position matrix and the driving signal. To measure the waves, a wave gauge system which consists of analog wave probes and a wave gauge monitor with a 16-bit A/D converter is used. The implementation of the wave generation and measurement part of the laboratory setup is complete and second-order regular and first-order irregular waves are tested.

A very common problem in laboratory wave generation is wave reflection. To mitigate the reflection waves in the wave flume, an energy-dissipating beach consisting of small-sized rocks are laid at the end of the channel at a 1:5 slope and substantial improvements are observed in the generated waves. Then, a reflection analysis is conducted using irregular wave measurements. The results revealed that the reflection is still influential in the wave flume although reflected waves occupying a smaller percentage of the total wave energy. For future works in this project, the active absorption method is aimed to be implemented in wave generation. However, the first challenge in the active absorption will be the implementation of an active feedback system between the real-time wave measurements and the driving signal that is sent to the AC motor of the wave generator.

The Froude scaling is applied to obtain the model of a spar-type floating platform. The dynamic similitude is achieved and the floating platform model and catenary mooring lines are constructed with properties derived from a 1:40 length scale. To retain the original symmetry of the mooring lines requires the tests to be conducted in a

large basin. However, the dimensions of the laboratory wave flume introduce limitations in the lateral axis. Thus, a compromise has been made to keep the original symmetry of the mooring lines at the platform location; a pulley system that lets the mooring cables traverse through is designed and produced. The pulleys, when mounted on the sidewalls of the wave flume close to the spar model, allows the mooring lines to retain their original symmetries from the spar model to the pulleys, the rest of the mooring line sections pass through the pulleys, and their direction changes to parallel to the longitude of the wave flume. For practical reasons, the pulleys are mounted on the sidewalls using industrial stainless magnets, which allows easier relocation when needed. Adopting this layout allows the mooring lines to tighten and loosen, according to the motion of the floating platform while preserving the original mooring line properties, yet, some energy loss due to friction is expected as the lines traverse through the pulleys. However, at this point, the measurement instruments for the cable tensions and platform time response are not implemented. As a future study, experiments will be conducted to measure the responses of the FOWT under various regular and irregular waves and results will be used to verify the numerical model study performed in this thesis.

REFERENCES

Alkarem, Yüksel. 2020. “Numerical Examination of Floating Offshore Wind Turbine and Development of an Innovative Floating Platform Design.”

Aqwa, Ansys. 2013. “Introduction to Hydrodynamic Analysis with Ansys Aqwa.” *Aqwa*, 1–32.

Barthel, V., E. P.D. Mansard, S. E. Sand, and F. C. Vis. 1983. “Group Bounded Long Waves in Physical Models.” *Ocean Engineering* 10 (4): 261–94. https://doi.org/10.1016/0029-8018(83)90012-4.

Biesel, F. 1951. “Etude Théorique d’un Certain Type d’appareil a Houle.” *La Houille Blanche* 2 (4): 475–96.

BNEF. 2018. “Global Offshore Wind Market Set to Grow Sixfold by 2030.” January 8. 2018. https://about.bnef.com/blog/global-offshore-wind-market-set-to-grow-sixfold-by-2030/.

Bouws, E., H. Gunther, W. Rosenthal, and C. L. Vincent. 1985. “Similarity of the Wind Wave Spectrum in Finite Depth Water 1. Spectral Form.” *Journal of Geophysical Research* 90 (C1): 975–86. https://doi.org/10.1029/JC090iC01p00975.

Bretschneider, C. L. 1959. *Wave Variability and Wave Spectra for Wind-Generated Gravity Waves. No. 118*. The Board.

Butterfield, Sandy, W Musial, Jason Jonkman, and Paul Sclavounos. 2005. “Engineering Challenges for Floating Offshore Wind Turbines.” *Offshore Wind Conference*, 13.

Chakrabarti, Subrata. 1995. “Offshore Structure Modelling.” *Applied Ocean Research* 17 (6): 391–92. https://doi.org/10.1016/s0141-1187(96)00012-0.

Dean, R. G., and R. A. Dalrymple. 1984. *Water Wave Mechanics for Engineers and Scientists.* https://doi.org/10.1029/eo066i024p00490-06.

Erol, Serkan. 2020. “SCALED DOWN MODELLING OF A HORIZONTAL WIND TURBINE FOR A FLOATING WIND TURBINE RESEARCH.”

Flick, Reinhard E., and Robert T. Guza. 1980. “Paddle Generated Waves in Laboratory Channels.” *Journal of the Waterway, Port, Coastal and Ocean Division, Proceedings of the American Society of Civil Engineers* 106 (1): 79–97.

Fontanet, Pierre. 1961. “Théorie de La Génération de La Houle Cylindrique Par Un Batteur Plan (2e Ordre d’approximation).” *Houille Blanche*, no. 1: 3–31. https://doi.org/10.1051/lhb/1961020.

Funke, E.R, E.P.D. Mansard, and G. Dai. 1988. “REALIZABLE WAVE PARAMETERS IN A LABORATORY FLUME.” In *21st International Conference on Coastal Engineering*, 835–48.

Gilbert, G., D. M. Thompson, and A. J. Brewer. 1971. *Design Curves for Regular and Random Wave Generators*. *Journal of Hydraulic Research*. Vol. 9. https://doi.org/10.1080/00221687109500345.

Goda., Yoshimi, and Yasumasa Suzuki. 1976. “Estimation of Incident and Reflected Waves in Random Wave Experiments.” *Ocean Engineering* 22 (1): 77–86. https://doi.org/10.1016/0029-8018(93)E0011-G.

Goda, Yoshimi. 1967. “Travelling Secondary Wave Crests in Wave Channels.”

———. 1970. “Numerical Experiments on Wave Statistics with Spectral Simulation.” *Report Port Harbour Res. Inst.* 9: 3–57. http://ci.nii.ac.jp/naid/10011190974/en/.

———. 1979. “A Review on Statistical Interpretation of Wave Data.” *Report of the Port and Harbour Research Institute*.

———. 1988. “Statistical Variability of Sea State Parameters as a Function of Wave Spectrum.” *Coastal Engineering in Japan* 31 (1): 39–52. https://doi.org/10.1080/05785634.1988.11924482.

———. 1999. “A Comparative Review on the Functional Forms of Directional Wave Spectrum.” *Coastal Engineering Journal* 41 (1–4): 1–20. https://doi.org/10.1142/s0578563499000024.

———. 2000. *Random Seas and Design of Maritime Structures*. *World Scientific*. Vol. 15.

GWEC. 2019. “Global Wind Report 2019.” 2019. https://gwec.net/global-wind-report/

Hasselmann, K. 1973. “Measurements of Wind-Wave Growth and Swell Decay during the Joint North Sea Wave Project (JONSWAP).” *Deutches Hydrographisches Institut*, no. Ergänzungsheft 8-12.

Havelock, T H. 1929. “LIX . Forced Surface-Waves on Water.” *The London, Edinburgh, and Dublin Philosophical Magazine and Journal of Science* 8 (51): 569–76. https://doi.org/10.1080/14786441008564913.

Huang, Norden E., Steven R. Long, Chi Chao Tung, Yeli Yuen, and Larry F. Bliven. 1981. “A Unified Two-Parameter Wave Spectral Model for a General Sea State.” *Journal of Fluid Mechanics* 112 (55): 203–24. https://doi.org/10.1017/S0022112081000360.

Hughes, Steven A. 1993. *Physical Models and Laboratory Techniques in Coastal Engineering*. *Advanced Series on Ocean Engineering*. Vol. Volume 7. WORLD SCIENTIFIC. https://doi.org/doi:10.1142/2154.

Hyun, Jae Min. 1976. “Simplified Analysis of a Plunger-Type Wavemaker Performance.” *Journal of Hydronautics* 10 (3): 89–94. https://doi.org/10.2514/3.63056.

Jonkman, J. 2010. “Definition of the Floating System for Phase IV of OC3.” *Contract* 1 (May): 31. https://doi.org/10.2172/979456.

Jonkman, J, and W Musial. 2010. “Offshore Code Comparison Collaboration (OC3) for IEA Task 23 Offshore Wind Technology and Deployment.” *IEA Task 23* 303 (December): 74. https://doi.org/NREL/TP-5000-48191.

Landberg, Lars. 2016. *Meteorology for Wind Energy*. https://doi.org/10.1002/9781118913451.

Mackay, E. B.L. 2012. *Resource Assessment for Wave Energy*. *Comprehensive Renewable Energy*. Vol. 8. Elsevier Ltd. https://doi.org/10.1016/B978-0-08-087872-0.00803-9.

Madsen, O. S. 1970. “Waves Generated by a Piston-Type Wavemaker.” *Coastal Engineering*, 589–607. https://doi.org/10.31826/9781463231699-040.

Madsen, O.S. 1971. “On the Generation of Long Waves.” *Coastal Engineering* 76 (36).

https://doi.org/10.1029/JC076i036p08672

Mansard, E. P.D. 1988. “Sub and Superharmonics in Natural Waves.” J*ournal of Offshore Mechanics and Arctic Engineering* 110 (3): 210–17. https://doi.org/10.1115/1.3257053.

Martin, Heather R., Richard W. Kimball, Anthony M. Viselli, and Andrew J. Goupee. 2014a. “Methodology for Wind/Wave Basin Testing of Floating Offshore Wind Turbines.” *Journal of Offshore Mechanics and Arctic Engineering* 136 (2): 021902. https://doi.org/10.1115/1.4025030.

———. 2014b. “Methodology for Wind/Wave Basin Testing of Floating Offshore Wind Turbines.” *Journal of Offshore Mechanics and Arctic Engineering* 136 (2): 020905. https://doi.org/10.1115/1.4025030.

Miles, M. D., and E. P. Funke. 1988. “NUMERICAL COMPARISON OF WAVE SYNTHESIS METHODS.” In *21st International Conference on Coastal Engineering*. https://ascelibrary.org/doi/pdf/10.1061/9780872626874.007.

———. 1989. “A Comparison of Methods for Synthesis of Directional Seas.” *Journal of Offshore Mechanics and Arctic Engineering* 111 (1): 43–48. https://doi.org/10.1115/1.3257137.

Mitsuyasu, H. 1970. “On the Growth of Wind-Generated Waves (2)-Spectral Shape of Wind Waves at Finite Fetch-.” *Proc. 17th Japanese Conf. Coastal Eng., 1970*. http://ci.nii.ac.jp/naid/10018957596/en/.

Newland, D. E. 2012. *An Introduction to Random Vibrations, Spectral & Wavelet Analysis*. Courier Corporation.

Newman, J. N. 1990. “Numerical Solutions of the Water-Wave Dispersion Relation.” *Applied Ocean Research* 12 (1): 14–18. https://doi.org/10.1016/S0141-1187(05)80013-6.

Ottesen-Hansen, N. E. 1978. “Long Period Waves in Natural Wave Trains.”

Ottesen-Hansen, N. E., Stig E Sand, H. Lundgren, Torben Sorensen, and H. Gravesen. 1980. “CORRECT REPRODUCTION OF GROUP-INDUCED LONG WAVES.” In *Coastal Engineering 1980*, 784–800.

Pierson, Willard J., and Lionel Moskowitz. 1964. “A Proposed Spectral Form for Fully Developed Wind Seas Based on the Similarity Theory of S. A. Kitaigorodskii.” *Journal of Geophysical Research* 69 (24): 5181–90. https://doi.org/10.1029/jz069i024p05181.

Samii, K., and J. K. Vandiver. 1984. “A Numerically Efficient Technique for the Simulation of Random Wave Forces on Offshore Structures.” *Proceedings of the Annual Offshore Technology Conference* 1984–May: 301–8. https://www.onepetro.org/conference-paper/OTC-4811-MS.

Sand, Stig E. 1982a. “Long Wave Problems in Laboratory Models.” *Journal of the Waterway, Port, Coastal and Ocean Division* 108 (4): 492-503.

———. 1982b. “Long Waves in Directional Seas.” *Coastal Engineering* 6 (3). https://doi.org/10.1016/0378-3839(82)90018-7.

Sand, Stig E., and Bjarne Donslund. 1985. “Influence of Wave Board Type on Bounded Long Waves.” *Journal of Hydraulic Research* 23 (2): 147–63. https://doi.org/10.1080/00221688509499362.

Sand, Stig E., and E. P.D. Mansard. 1986. “Reproduction of Higher Harmonics in Irregular Waves.” *Ocean Engineering* 13 (1): 57–83. https://doi.org/10.1016/0029-8018(86)90004-1.

Schaffer, H. a., and K. P. Jakobsen. 2003. “Non-Linear Wave Generation and Active Absorption in Wave Flumes.” *Long Waves Symposium*, no. January 2003: 69–76.

Schäffer, Hemming A. 1994. “Second Order Irregular-Wave Generation in Flumes - Computation of Transfer Functions by an Asymptotic Summation Method.” In , 784–97.

———. 1996. “Second-Order Wavemaker Theory for Irregular Waves.” *Ocean Engineering* 23 (1): 47–88. https://doi.org/10.1016/0029-8018(95)00013-B.

Schäffer, Hemming A., and Cathrine M Steenberg. 2003. “SECOND-ORDER WAVE GENERATION IN LABORATORY BASSINS.” *Ocean Engineering* 30 (10): 1203–31.

Snyder, Brian, and Mark J. Kaiser. 2009. “Ecological and Economic Cost-Benefit

Analysis of Offshore Wind Energy." *Renewable Energy* 34 (6): 1567–78. https://doi.org/10.1016/j.renene.2008.11.015.

Spinneken, Johannes, and Chris Swan. 2009a. "Second-Order Wave Maker Theory Using Force-Feedback Control. Part I: A New Theory for Regular Wave Generation." *Ocean Engineering* 36 (8): 539–48. https://doi.org/10.1016/j.oceaneng.2009.01.019.

———. 2009b. "Second-Order Wave Maker Theory Using Force-Feedback Control. Part II: An Experimental Verification of Regular Wave Generation." *Ocean Engineering* 36 (8): 549–55.

Stokes, G. G. 1880. "On the Theory of Oscillatory Waves." *Transactions of the Cambridge Philosophical Society*. http://ci.nii.ac.jp/naid/10010286911/en/.

Sulisz, W., and R. T. Hudspeth. 1993. "Complete Second-Order Solution for Water Waves Generated in Wave Flumes." *Journal of Fluids and Structures*. https://doi.org/10.1006/jfls.1993.1016.

Tuah, Hang, and Robert T. Hudspeth. 1982. "Comparisons of Numerical Random Sea Simulations." *Journal of the Waterway, Port, Coastal and Ocean Division* 108 (4): 569–84. https://cedb.asce.org/CEDBsearch/record.jsp?dockey=0034804.

Ursell, F., R. G. Dean, and Y. S. Yu. 1960. "Forced Small-Amplitude Water Waves: A Comparison of Theory and Experiment." *Journal of Fluid Mechanics* 7 (1): 33–52. https://doi.org/10.1017/S0022112060000037.

Wallingford, H. R. 2015. *Wave Gauge System User Manual*.

Wang, H. T., and J. D. Crouch. 1993. "Accuracy of Low-Order Models for Simulations of Random Ocean Waves." *Journal of Waterway, Port, Coastal, and Ocean Engineering* 119 (1): 70–87. https://doi.org/https://doi.org/10.1061/(ASCE)0733-950X(1993)119:1(70).

Wang, Shen. 1974. *Plunger-Type Wavemakers: Theory And Experiment*. *Journal of Hydraulic Research*. Vol. 12. https://doi.org/10.1080/00221687409499732.

Wu, Yung Chao. 1988. "Plunger-Type Wavemaker Theory." *Journal of Hydraulic Research* 26 (4): 483–91. https://doi.org/10.1080/00221688809499206.